CHARACTERIZING PHYSICOCHEMICAL AND THERMOMECHANICAL BEHAVIOR OF COLLAGEN-BASED SCAFFOLDS FOR BONE MARROW TISSUE ENGINEERING

Ifeoluwa Adeniyi

A THESIS SUBMITTED TO THE FACULTY OF GRADUATE STUDIES IN PARTIAL FULFILLMENT OF THE REQUIREMENTS FOR THE DEGREE OF MASTER OF APPLIED SCIENCE

GRADUATE PROGRAM IN MECHANICAL ENGINEERING

YORK UNIVERSITY

TORONTO, ONTARIO

SEPTEMBER 2026

© Ifeoluwa Adeniyi, 2026

Abstract

Collagen is widely used in tissue engineering because it is biocompatible, mechanically tunable, and can mimic native extracellular matrix (ECM) environments. However, implantable biomaterials must meet mandated ISO sterilization requirements, and depending on the technique, these processes can alter collagen's structural and mechanical properties. While cellular responses to ionizing radiation are well documented, its effects on ECM structure and mechanics remain underexplored. This study examined how X-ray sterilization and crosslinking influence the denaturation temperature, spectroscopy, elastic behavior, and degradation kinetics of 2D collagen films. Eight experimental conditions were tested across collagen-only and composite materials, comparing non-crosslinked vs. crosslinked and ethanol-sterilized vs. 25 kGy-irradiated states. DSC, DMA, FTIR, and degradation assays quantified thermomechanical and chemical changes. A secondary objective assessed batch-to-batch variability to determine whether limited tests could predict degradation, elasticity, and spectral features, enabling adjustments in crosslinking. Findings show that irradiation and crosslinking significantly affect scaffold stability and performance.

Graphical Abstract: The Impact of Collagen-Source Variability and Post-Processing on Collagen Scaffold Properties.

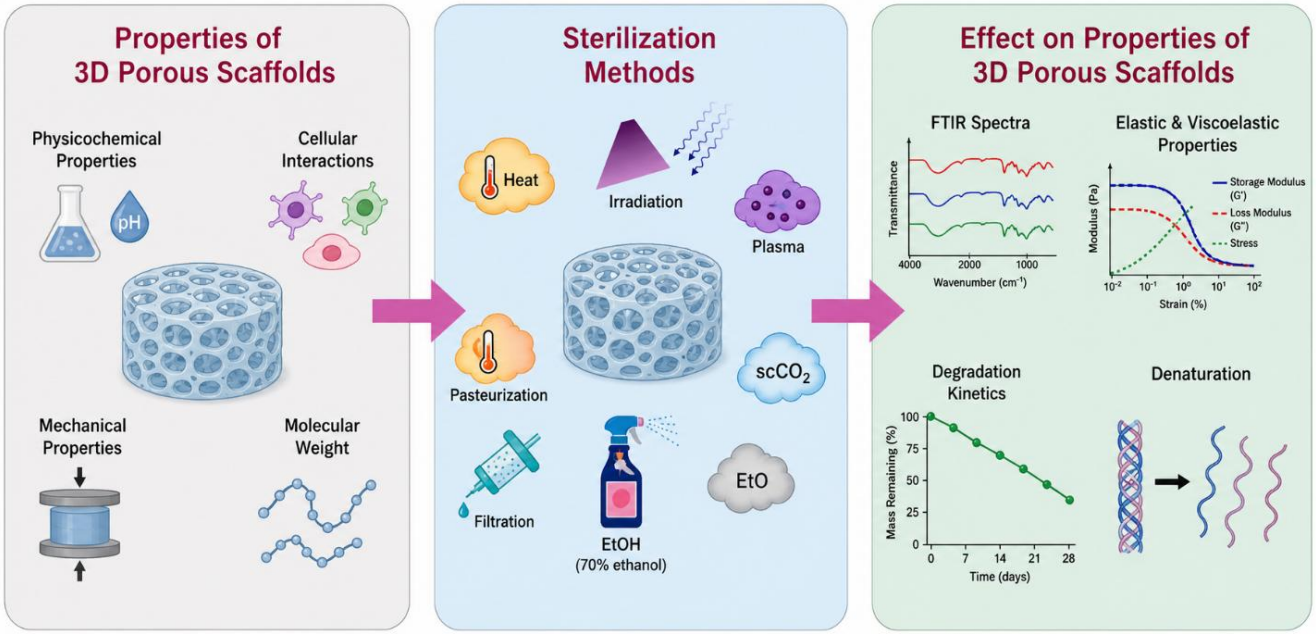

Acknowledgements

I would like to express my deepest gratitude to God. I am also profoundly thankful to my parents for their unwavering financial and emotional support throughout my academic journey. Their encouragement, patience, and steadfast belief in my abilities made it possible for me to pursue and complete this work.

I would also like to thank my Principal Investigator, Dr. Terry Sachlos, for his mentorship, guidance, patience, and support throughout this research.

I am sincerely grateful to all members of the lab for their training, guidance, technical support, and willingness to help throughout this project. I especially wish to thank Farrah, Milad, Adriana, and Joab for their generous assistance, advice, and support.

This work was supported by funding from the Collaborative Health Research Projects (CHRP) program, the Natural Sciences and Engineering Research Council of Canada (NSERC), Connected Minds, and the Canada Foundation for Innovation (CFI). I gratefully acknowledge these organizations for supporting the research environment and resources that made this work possible.

Finally, I would like to thank York University for providing the opportunity, facilities, and academic environment in which this research was completed.

Table of Contents

Abstract ii

Graphical Abstract: The Impact of Collagen-Source Variability and Post-Processing on Collagen Scaffold Properties. iii

Acknowledgements iv

Table of Contents v

List of Figures viii

Chapter 1: Introduction 1

Hypothesis 7

Aim 1: Characterize the physicochemical and mechanical properties of collagen-based scaffolds across batches 7

Aim 2: Establish a standardized method to estimate mechanical properties from limited physicochemical testing 7

Chapter 2: Literature Review 9

2.1 The Extracellular Matrix 10

2.2 Scaffold design requirements 12

2.2.1 Microarchitecture 12

2.2.2 Biodegradability 12

2.2.3 Biocompatibility 13

2.2.4 Mechanical properties 13

2.3 Scaffold materials 14

2.3.1 Ceramics 14

2.3.2 Polymers 16

2.3.3 Metals 21

2.4 Scaffold Manufacturing 21

2.4.1 Particulate Leaching 22

2.4.2 Freeze drying 23

2.4.3 Electrospinning 24

2.4.4 Gas foaming 24

2.4.5 Thermal-Induced Phase Separation 25

2.5 Crosslinking Techniques 25

2.6 Sterilization techniques 29
2.7 Characterization 31
Chapter 3: Materials and Methods 34
3.1 Collagen Slurry Preparation 35
3.2 2D Scaffold Preparation 35
3.3 X-ray Sterilization 36
3.4 Crosslinking 36
3.5 Experimental groups 37
3.6 Differential Scanning Calorimetry 38
3.7 Rheological testing 39
3.8 Fourier Transform Infrared Spectroscopy (FTIR) 40
3.9 Collagenase degradation 41
3.10 Statistical analysis 42
Chapter 4: Results 43
4.1 Molecular Characterization 44
4.2 Thermal Property Characterization 48
4.3 Elastic behavior results 51
4.4 Enzymatic degradation of type 1 collagen 54
4.4.1 Preliminary 5-day Degradation results 54
4.4.2 24-hour time-resolved degradation experiment 56
Chapter 5: Discussion 61
5.1 Molecular analysis 62
5.1.1 Collagen scaffolds 62
5.1.2 Composite scaffolds 63
5.2 Thermal property analysis 65
5.2.1 Effect of Irradiation on the scaffold 65
5.2.2 Effect of crosslinking within each composition and sterility state 66
5.2.3 Combined Effect of irradiation and crosslinking 67
5.3 Elastic behavior 68
5.4 Enzymatic degradation 69
5.5 Streamlined physicochemical and thermomechanical assessment 70

5.6 Limitations of the study 71
Chapter 6: Batch-to Batch Variability 73
6.1 Degradation behaviour 75
6.2 Degradation mechanism 76
6.3 Mechanical and thermal properties 78
6.4 Relationships among endpoints 79
6.5 Batch transferability and Performance Index 80
Chapter 7: Conclusion and Future Work 83
References 86

List of Figures

Figure 1.1: Stem cells reside in microenvironments that span a broad mechanical spectrum, ranging from the marrow's near-fluid softness (<1 kPa) to the extreme rigidity of mineralized bone in the gigapascal range. Micro-elasticity generally increases with collagen abundance across tissues, yet even the stiffest native niches remain markedly more compliant than conventional rigid plastic substrates used for in vitro culture. Adapted from [6] 3

Figure 1.2: Illustration of the tissue-engineering cycle, beginning with the collection of a patient biopsy to obtain the necessary cell population. The harvested cells are expanded and combined with a biomaterial scaffold engineered to mimic key structural and biochemical features of the native extracellular matrix. Bioactive factors, such as growth factors, cytokines, or hormones, are introduced to guide cell proliferation, differentiation, and matrix deposition. Following maturation, the engineered construct is implanted back into the patient, where it integrates with host tissue, supports regeneration, and ultimately remodels into functional native tissue. 4

Figure 2.1: Schematic representation of the tissue-engineering triad, illustrating the three essential components required for functional regeneration: cells, which provide the biological drivers of repair; scaffolds, which supply structural and biochemical support; and signaling cues, encompassing growth factors and environmental stimuli that direct cell behavior. Together, these elements form the foundational framework for engineered tissue development. 11

Figure 2.2: Materials used for scaffold development. Materials are divided into three broad categories. A few examples of each classification are provided. 15

Figure 2.3: Schematic overview of conventional fabrication techniques used to generate porous polymeric scaffolds for tissue engineering applications. The diagram illustrates five widely employed methods—freeze drying, electrospinning, thermal-induced phase separation, solvent

casting and particle leaching, and gas foaming—each highlighting the sequential processing steps that govern pore formation, structural morphology, and final scaffold architecture, adapted from[65] 23

Figure 2.4: Schematic representation of three major cross-linking strategies used to stabilize type I collagen scaffolds. Physical cross-linking methods include UV irradiation and dehydrothermal treatment. Chemical cross-linking involves carbodiimide chemistry (EDC/NHS) to activate carboxyl groups to form covalent linkages within the collagen network. Biological cross-linking uses naturally derived agents such as genipin to generate stable amide bonds. Adapted from[70] . 27

Figure 3.1: Schematic representation of collagen powder swelling and homogenization process. 35

Figure 3.2: Schematic representation of the sterilization and crosslinking of the collagen-based 2D scaffolds. 36

Figure 3.3: Hierarchical organization of scaffold groups and experimental conditions used in this study. Scaffold types are categorized into collagen and composite formulations, each further subdivided into irradiated and non-irradiated variants. Within each irradiation condition, scaffolds are classified as crosslinked or non-crosslinked, forming the full matrix of experimental groups subjected to downstream characterization. All scaffold variants undergo thermomechanical testing, secondary structure analysis, and collagenase degradation analysis to evaluate thermal stability, structural integrity, and enzymatic susceptibility. 38

Figure 4.1: FTIR spectra of collagen-only scaffolds in the fingerprint region (1800–600 cm^{-1}). Normalized absorbance spectra are shown for non-irradiated un-crosslinked (N_IR-UCL), non-irradiated crosslinked (N_IR-XL), irradiated un-crosslinked (IR-UCL), and irradiated crosslinked (IR-XL) collagen scaffolds. Key collagen vibrational bands are indicated, including

the C=O stretch (~1772 cm^{-1}), Amide I, Amide II, CH_2 bending, COO symmetric stretch, Amide III, and C–O (~1080 cm^{-1}). Crosslinking produced minor shifts in the amide bands, consistent with increased molecular packing. At the same time, sterilization resulted in pronounced downshifts and reduced Amide III intensity, indicating partial denaturation of the collagen triple helix..... 45

Figure 4.2: ATR FTIR spectra of collagen–hydroxyapatite–elastin composite scaffolds under four fabrication condition: non-irradiated un-crosslinked (N_IR-UCL), non-irradiated crosslinked (N_IR-XL), irradiated un-crosslinked (IR-UCL), and irradiated crosslinked (IR-XL) composite scaffolds. Spectra display characteristic protein bands (Amide A ~3286–3288 cm^{-1}, Amide I 1631–1641 cm^{-1}, Amide II 1529–1549 cm^{-1}, Amide III 1232 cm^{-1}), elastin-associated C–H deformation (1444–1448 cm^{-1}), and hydroxyapatite phosphate modes (ν_3 PO_4^{3-} at 1024–1028 and 1072–1090 cm^{-1}; ν_1 PO_4^{3-} at 960–978 cm^{-1}; ν_4 PO_4^{3-} at 560 and 600 cm^{-1}) and the OH^- liberation band (625–635 cm^{-1}). The persistence of ν_3 and ν_4 doublets and the OH^- band confirms the presence of crystalline hydroxyapatite across all conditions. 46

Figure 4.3: DSC Thermograms for the collagen and composite scaffold across the 4 processing conditions. (a) Thermograms for collagen-only film scaffolds processed under four conditions: N_IR-UCL (non-irradiated, un-crosslinked; yellow), N_IR-XL (non-irradiated, crosslinked; blue), IR-UCL (irradiated, un-crosslinked; red), and IR-XL (irradiated, crosslinked; green). Curves illustrate the characteristic endothermic transition associated with collagen denaturation and highlight shifts in thermal stability as a function of irradiation and crosslinking. (b) Corresponding DSC thermograms for composite scaffolds under the same four processing conditions, plotted using the identical color scheme and abbreviations. 49

Figure 4.4: Denaturation temperature of collagen-only and composite scaffolds under four processing conditions. Box-and-whisker plots show the distribution of denaturation temperature (Td) values for collagen-only and composite scaffolds across four processing conditions combining sterility and crosslinking, yielding a total of eight groups (n=3). Each box represents the interquartile range with the median indicated, and whiskers denote the full data range. 50
Figure 4.5: Mechanical properties of collagen and composite 2D films under different sterilization and crosslinking conditions. (a) Ultimate tensile strength (UTS) of collagen films as mean ± standard deviation. (b) Elastic moduli of collagen films presented as mean ± standard deviation. (c) Representative stress-strain curves of collagen films under four conditions: N_IR-UCL (non-irradiated, un-crosslinked, Blue), N_IR-XL (non-irradiated, crosslinked, Red dotted), N_IR-UCL (irradiated, un-crosslinked, Orange), and IR-XL (irradiated, crosslinked, Black dotted). (d) Representative stress-strain curves of composite films under the same four conditions. (e) Ultimate tensile strength (UTS) of composite films as mean ± standard deviation. (f) Elastic moduli of composite films presented as mean ± standard deviation. Statistical significance is indicated where applicable ($p < 0.005$); n = 3 for all groups. 52
Figure 4.6: Enzymatic degradation of collagen-based scaffolds over five days. (a) Percentage of mass remaining for all sterile scaffolds and non-sterile composite scaffolds following incubation in collagenase for five days. (b) Percentage of collagen degraded in composite scaffolds across all four processing conditions (sterile crosslinked, sterile un-crosslinked, non-sterile crosslinked, non-sterile un-crosslinked). Values are normalized to the initial collagen content of each composite scaffold. Data represent n = 2, shown as mean ± SD. 55
Figure 4.7: In vitro enzymatic degradation of collagen-based scaffolds over 24 hours. (a) Percentage of mass remaining for collagen-only scaffolds under four processing conditions:

N_IR-UCL (non-irradiated, un-crosslinked; yellow), N_IR-XL (non-irradiated, crosslinked; blue), IR-UCL (irradiated, un-crosslinked; orange), and IR-XL (irradiated, crosslinked; green). (b) Percentage of bulk mass remaining for composite scaffolds under the same four conditions. For panels (a) and (b), solid lines represent a non-linear regression fit using a first-order, one-phase exponential decay model constrained to a baseline of 100% and a plateau of 0%. (c) Percentage of collagen-normalized mass remaining for composite scaffolds under the same four processing conditions. Experimental data represent mean ± SD (n = 3). Solid lines represent a non-linear regression fit using a first-order, one-phase exponential decay model constrained to a baseline of 100% and a plateau of 50%. (d) Composite control samples incubated in Tris buffer containing 5 mM $CaCl_2$, washed after 1 hour and 24 hours, shown for crosslinked (red) and un-crosslinked (blue) scaffolds (n = 3). 59

Figure 6.1: Composite scaffold degradation during collagenase exposure. Total mass remaining of composite scaffolds from batches 1 and 2: Composite scaffold degradation during collagenase exposure. Total mass remaining of composite scaffolds from batches 1 and 2: (A) non-irradiated, un-crosslinked (N_IR-UCL); (B) non-irradiated, crosslinked (N_IR-XL); (C) irradiated, un-crosslinked (IR-UCL); and **(D)** irradiated, crosslinked (IR-XL). Open symbols and dotted line segments indicate the 24 h observations. These measurements were excluded from the primary 3–12 h analysis because batch-2 specimens had a higher starting mass, resulting in a reduced enzyme: substrate ratio. The shaded region indicates the nominal 50% HA/elastin fraction of the composite scaffold. 76

Figure 6.2: Integrated decision map of scaffold performance and batch reproducibility. Scaffold Performance Index (SPI) is plotted against the Batch Reproducibility Index (BRI) for collagen-only and collagen–HA/elastin composite scaffolds. Higher SPI values indicate stronger overall

performance across the available endpoints, whereas higher BRI values indicate closer agreement between batches. Dashed lines indicate median thresholds used to define the performance and reproducibility quadrants. The blue shaded upper-right quadrant identifies conditions that combine above-median scaffold performance with above-median batch reproducibility. 81

Chapter 1: Introduction

While organ transplantation has become the benchmark treatment for patients with end-stage organ failure, the availability of donor tissue has not kept pace, creating an imbalance between supply and demand. Although advances in surgical techniques and post-transplant care have significantly reduced mortality during and post-surgery, the persistent shortage of donors continues to limit patients' access to life-saving therapies. It remains one of the major challenges in medicine.

Although solid organ transplants of the heart, liver, lungs and kidney dominate clinical focus due to their high prevalence, the demand for Bone Marrow Transplantation (BMT) has risen steadily. This increase is driven by an aging population and the growing number of patients with hematological disorders, including acute myeloid leukemia, for which bone marrow transplantation remains the most effective and often the only curative therapy[1].

Despite its importance, bone marrow transplantation faces a unique and severe donor shortage. BMT requires a highly specific human leukocyte antigen (HLA) match between the donor and recipient. However, only an estimated 25-30% of patients can match with a suitable donor within their family, leaving the remaining 70-75% dependent on finding an unrelated donor in the registries[1].

To address this challenge, there is a growing need to shift from donor-dependent therapies to engineered biological solutions. Tissue engineering and regenerative medicine have emerged as promising strategies to overcome the constraints of donor availability through the development of biomimetic systems that replicate the structure and function of the damaged native tissues[2]. By designing scaffolds that mimic the biochemical composition and mechanical properties of the various cell niches, it may be possible to support cell proliferation, differentiation, and long-term function in vitro and eventually in vivo[3].

The extracellular matrix (ECM) of a cell is the dynamic microenvironment in which cells in their native tissues are embedded.[4]. While a structural unit, the ECM regulates factors that provide essential biochemical, biophysical, and biomechanical cues that direct cell fate, including but not limited to stem cell survival, self-renewal, and lineage commitment[4–7]. Among these cues, matrix stiffness has emerged as the most influential factor directing stem cell fate through mechano-transduction pathways that translate physical forces into intracellular signalling[6,8].

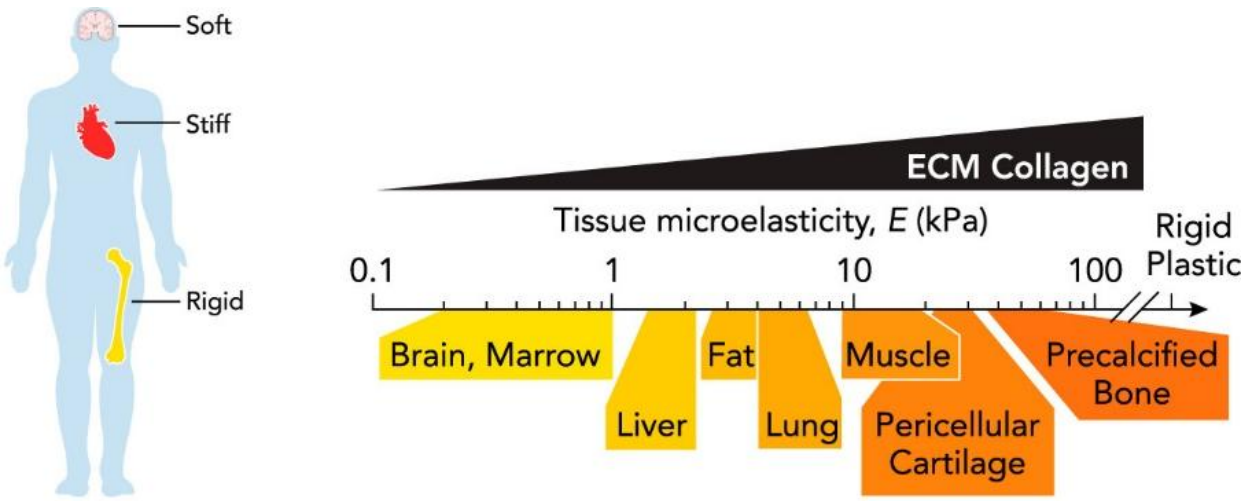

Figure 1.1.1: Stem cells reside in microenvironments that span a broad mechanical spectrum, ranging from the marrow's near-fluid softness (<1 kPa) to the extreme rigidity of mineralized bone in the gigapascal range. Micro-elasticity generally increases with collagen abundance across tissues, yet even the stiffest native niches remain markedly more compliant than conventional rigid plastic substrates used for in vitro culture. Adapted from [6]

Tissues across the body span a wide mechanical spectrum-from the extremely soft brain tissue with Young's moduli of < 1 kPa, to bone, which reaches the gigapascal range- creating distinct mechanical microenvironments that guide stem cell lineage commitment[6–8]. Soft matrices resembling neural tissue promote neurogenic outcomes, whereas medial stiffness supports myogenic differentiation and rigid matrices drive osteogenic lineage commitment[6,8], Figure 1.1. These patterns reflect how stem cells interpret mechanical cues through integrins, cytoskeletal

tension, and mechanosensitive regulators such as YAP/TAZ and piezo-type ion channels, which move between the cytoplasm and nucleus in response to changes in matrix rigidity[9,10]. Therefore, while a multitude of factors influence stem cell lineage, including growth factors, ECM composition, and cell-to-cell interactions, the ECM exerts most of its influence through biomechanical regulation, with stiffness as its primary signal that directs stem cell fate[4,9,11].

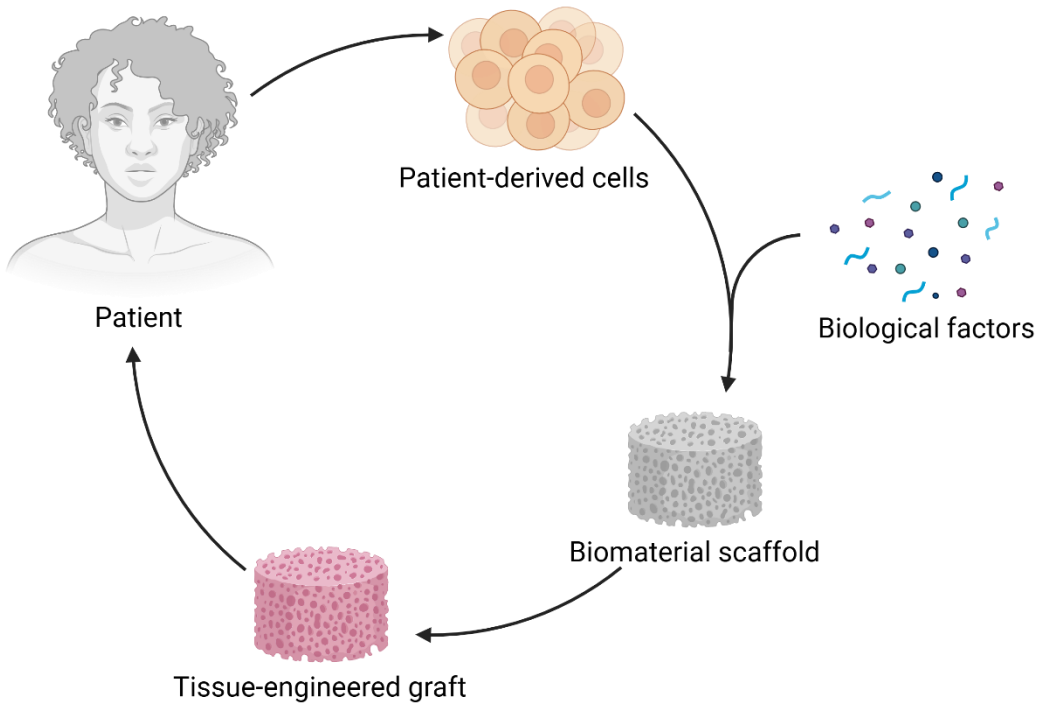

Figure 1.1.2: Illustration of the tissue-engineering cycle, beginning with the collection of a patient biopsy to obtain the necessary cell population. The harvested cells are expanded and combined with a biomaterial scaffold engineered to mimic key structural and biochemical features of the native extracellular matrix. Bioactive factors, such as growth factors, cytokines, or hormones, are introduced to guide cell proliferation, differentiation, and matrix deposition. Following maturation, the engineered construct is implanted back into the patient, where it integrates with host tissue, supports regeneration, and ultimately remodels into functional native tissue.

Tissue engineering builds upon this fundamental understanding of cell–matrix interactions by integrating three essential components: a suitable cell source, a biocompatible scaffold, and

signaling molecules that regulate cellular behavior[2,3,12]. The process typically begins with the isolation of cells from autologous, allogeneic, or xenogeneic sources, often obtained through a biopsy[3]. These cells are then expanded in culture—commonly within controlled bioreactor systems that provide optimal conditions for proliferation and phenotype maintenance[3,13,14]. Once an optimal amount is achieved, the cells are seeded onto a scaffold designed to mimic the physical and biochemical properties of the native extracellular matrix[2,3,14]. Within this engineered environment, cells continue to grow and differentiate, ultimately forming a functional tissue construct. The matured construct can then be implanted into the host to restore, replace, or regenerate diseased, damaged, or worn-out tissue[3,15].

Once implanted, the scaffold integrates with the host tissue, supporting cell adhesion, migration, and matrix deposition to promote self-repair[12]. Over time, the biomaterial is expected to biodegrade at the rate of new tissue formation to be replaced by the newly synthesized native ECM, restoring long-term tissue function. Although the choice of cell source, soluble regulatory factors, and biomaterial chemistry are all critical, successful regeneration ultimately depends on whether the scaffold reproduces the mechanical properties of the target tissue[3,12]. If the stiffness of the engineered construct does not match its physiological requirements, cell behavior becomes dysregulated, integration is impaired, and the implant is at risk of failure[2,3,16]. Thus, replicating the biomechanical environment, particularly tissue-specific stiffness, is essential for engineered scaffolds to guide appropriate stem cell responses and achieve durable regeneration.

Among the available biomaterials for degradable scaffold development, collagen—the most abundant protein in the human body—is widely used in bone tissue engineering and regenerative medicine because its structure and tunable properties enable it to mimic key features of the native extracellular matrix (ECM), including mechanical cues such as stiffness[2,15,17]. Comprising

approximately 90% of the organic content in bone ECM, collagen's triple helix structure—formed by three intertwined polypeptide chains—provides a robust scaffold that supports cell adhesion, proliferation, and differentiation, making it ideal for recreating biomimetic environments in bone marrow tissue regeneration[15].

Despite these advantages, native type I collagen exhibits poor thermomechanical stability, with denaturation occurring at temperatures only slightly above physiological levels[18,19]. This thermal sensitivity limits its durability in clinical applications, particularly in load-bearing environments where mechanical integrity is critical[18]. To address this limitation, crosslinking techniques are commonly employed to reinforce collagen scaffolds, enhancing their mechanical strength, thermal stability, and resistance to enzymatic degradation[19,20].

In accordance with ISO standards, all medical devices—including collagen-based scaffolds, films, and hydrogels—must undergo sterilization to ensure patient safety[21,22]. However, sterilization methods such as gamma and X-ray irradiation can significantly alter the molecular structure of collagen[21,23,24]. While certain irradiation conditions may induce covalent crosslinking and improve stability, they can also cause structural damage, including chain scission, fragmentation, and loss of mechanical integrity[24–26].

This study investigates the interplay between X-ray sterilization and crosslinking in collagen-based scaffolds to optimize structural and mechanical properties without compromising biocompatibility. By elucidating how sterilization influences scaffold mechanics—and how crosslinking may mitigate these effects—this work seeks to inform the design of mechanically robust scaffolds capable of supporting appropriate mechano-transduction in bone tissue engineering.

Hypothesis

Physicochemical measurements of collagen-based scaffolds can be used to predict their mechanical performance and to quantify the property changes induced by crosslinking and irradiation. By establishing these relationships across multiple collagen batches, it should be possible to distinguish processing effects from material variability and to determine how crosslinking conditions should be adjusted on a batch-specific basis to achieve consistent scaffold performance.

Aim 1: Characterize the physicochemical and mechanical properties of collagen-based scaffolds across batches

1. Fabricate collagen-based scaffolds under a range of relevant processing conditions.
2. Characterize the spectral, thermal, structural, and mechanical properties of each scaffold formulation to build a comprehensive dataset.
3. Compare thermomechanical and degradation properties across batches to identify consistent trends or batch-dependent variability under identical processing conditions.

Aim 2: Establish a standardized method to estimate mechanical properties from limited physicochemical testing

1. Identify which physicochemical measurements correlate most strongly with the mechanical properties measured across scaffold batches.

2. Develop a standardized relationship or predictive approach that allows mechanical performance to be estimated from these limited measurements, without requiring full mechanical testing.

3. Evaluate the accuracy and batch-dependent limitations of this estimation approach, and outline the additional batches or validation needed to strengthen its reliability for broader application.

Chapter 2: Literature Review

2.1 The Extracellular Matrix

The extracellular matrix (ECM) provides the structural and biochemical framework that regulates cell behavior in native tissues[27]. It is an organized fibrous network comprised mainly of polymeric structural proteins such as collagen and elastin, glycoproteins, proteoglycans, and mineralized hydroxyapatite, mainly found in bone, among others[27]. Collagen fibers and hydroxyapatite provide tensile strength, elastin provides elasticity, and glycoproteins such as fibronectin and laminin mediate cell adhesion and signaling[27,28]. Collectively, these components create a dynamic microenvironment that determines cell fate while also providing mechanical integrity and organizing the microarchitecture[27,28].

Cells continuously sense and respond to the mechanical properties of their surrounding matrix through a process called mechanotransduction[10,28,29]. Through this process, cells convert mechanical cues into biochemical signals that regulate gene expression and cell fate[10,28]. Substrate stiffness, surface topography, and matrix viscoelastic properties each influence/regulate cytoskeletal organization, integrin clustering and other focal adhesion molecule dynamics, and downstream signaling pathways such as Yes-associated protein (YAP) and transcriptional coactivator with PDZ-binding motif (TAZ), ultimately shaping cell morphology, proliferation, and lineage commitment[9,10,27,28].

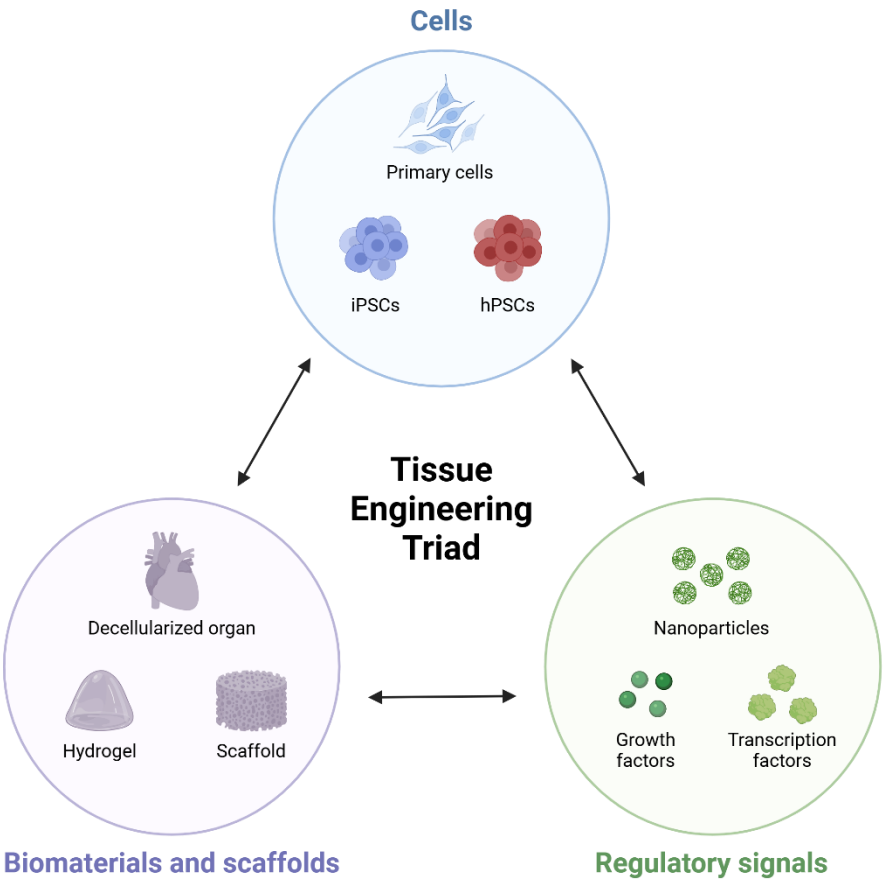

Figure 2.1: Schematic representation of the tissue-engineering triad, illustrating the three essential components required for functional regeneration: cells, which provide the biological drivers of repair; scaffolds, which supply structural and biochemical support; and signaling cues, encompassing growth factors and environmental stimuli that direct cell behavior. Together, these elements form the foundational framework for engineered tissue development.

Consequently, biomaterial scaffolds intended to replace or regenerate new tissue must be engineered to not only provide structural support but also to provide the appropriate mechanical cues that support the physiologically relevant mechano-transduction signaling[27,30].

Tissue engineering integrates 3 fundamental components- cells, signaling factors, and scaffolds- to restore, replace, or enhance tissue function[12]. The interplay between these elements is critical to ensure the implanted tissue functionality (Figure 2.1). Although the choice of cell source and

signaling factors is critical, successful regeneration ultimately depends on whether the scaffold reproduces the mechanical properties of the target tissue for implantability[28,31,32].

2.2 Scaffold design requirements

Tissue engineering scaffolds function as temporary templates that support the adhesion of cells, their migration, proliferation, and differentiation to guide tissue formation. Scaffold design depends on a multitude of factors, including microarchitecture, biodegradability, biocompatibility, and effective mechanical properties[12].

2.2.1 Microarchitecture

The microarchitecture must consider overall porosity, individual pore size, and interconnectivity, which influence nutrient and oxygen diffusion and cell infiltration[27]. Studies have shown that relatively small pores—on the order of 75–100 μm—are suitable for in vitro culture, whereas larger pores, typically between 200 and 500 μm, are more favorable in vivo because they facilitate deeper tissue penetration and improved vascularization[12]. High overall porosity further enhances cell–cell communication and promotes seamless integration between the engineered construct and the surrounding host tissue[12,32]. Supporting studies reported that scaffolds perform optimally when more than 60% of the pore population falls within the 150–400 μm range, with an additional fraction of smaller pores (<20 μm) contributing to overall network complexity and mass transport[32].

2.2.2 Biodegradability

This ensures that the gradual scaffold resorption and replacement by native tissue is at a rate synchronized to the healing process[12,27,33]. Because scaffolds function as a temporary support for

developing tissues, they will gradually break down once implanted through various chemical and enzymatic processes[12]. For optimal regeneration, the degradation profile of the scaffold should be directly proportional to the pace of new tissue formation[12]. While regenerating, the newly formed tissue replaces the scaffold through a process known as creeping substitution[34]. As the material degrades, its by-products should be non-toxic, easily metabolized, or safely cleared from the body without disrupting surrounding organs or interfering with physiological functions[12,32].

2.2.3 Biocompatibility

Biocompatibility minimizes immune reactions and promotes normal cellular response[12]. The chosen scaffold material should not trigger significant or chronic immune responses, as prolonged inflammation can impair healing, leading to implant failure. Any inflammatory activity that occurs should be resolved ideally within a short period of approximately 2 weeks so that normal tissue repair processes can proceed, ensuring regeneration[12].

2.2.4 Mechanical properties

The mechanical properties must closely match those of the target tissue at the intended implantation site, maintaining structural integrity under physiological loading to provide the appropriate mechanical cues for cellular behavior[2,12,28]. Because different tissues possess distinct mechanical characteristics, matching these properties is essential for maintaining structural support, preserving anatomical shape, and preventing complications such as stress shielding or secondary fractures[35]. Key mechanical parameters commonly evaluated in scaffold design include elastic modulus, tensile strength, fracture toughness, fatigue resistance, and elongation at break; all of which collectively determine the material's ability to perform reliably under physiological loading conditions[35–37].

2.3 Scaffold materials

The selection of materials dictates the scaffold's performance, influencing not only the mechanical integrity of the construct but also its biological interactions, degradation profile, and overall capacity to support functional tissue regeneration. Broadly, scaffold materials are categorized into ceramics, polymers (natural and synthetic), and metals, each offering distinct advantages and limitations. Increasingly, research has focused on combining these material classes to create composite scaffolds that better replicate the complexity of native tissues.

2.3.1 Ceramics

Ceramic materials represent a class of materials that are characterized by their high compressive strength, corrosion resistance, osteo-conductivity, and favorable interactions with biological environments[38–41]. These properties make ceramics particularly suitable for bone regeneration, where mechanical stiffness and mineral integration are essential[39]. These materials can be broadly categorized as bioinert, bioactive, and bioresorbable ceramics[39,41].

Bioinert ceramics such as alumina and zirconia are characterized by their chemical stability and minimal reactions with tissue environments[39]. Their wear resistance properties and high compressive strength make them appropriate for load-bearing applications such as joint replacement implants; however, their lack of bioactivity limits direct bonding with bone and limits their use in regenerative scaffolds[39].

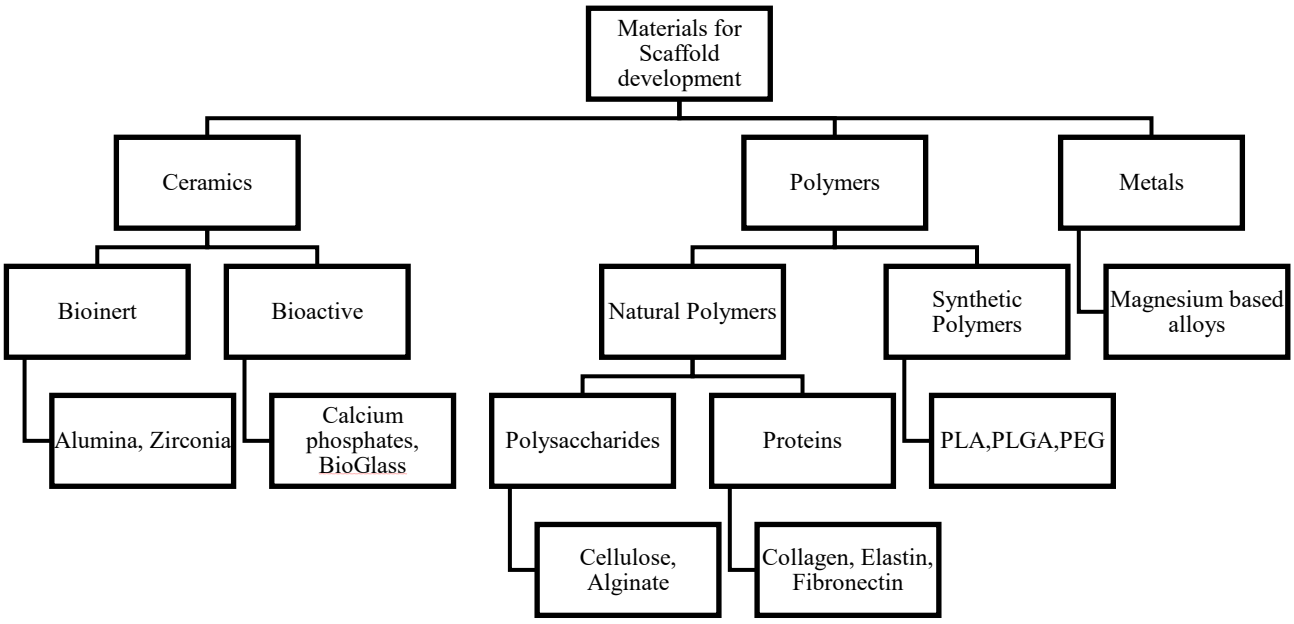

Figure 2.2: Materials used for scaffold development. Materials are divided into three broad categories. A few examples of each classification are provided.

In contrast, bioactive ceramics such as bio-glass and calcium phosphate-based materials (tri-calcium phosphate, Biphasic Calcium Phosphate, and hydroxyapatite) actively interact with biological systems[38,39]. Bio-glass, composed primarily of silica-based networks, is known for its ability to form layers of hydroxycarbonate apatite after implantation, which facilitates bonding with bone[38,39]. While degrading, it releases ionic products that can stimulate cellular activity and enhance osteogenesis. Despite these advantages, bio-glass tends to suffer from brittleness and limited mechanical reliability under load-bearing conditions, and its degradation profile can be difficult to control precisely[38].

Among bio-ceramics, calcium phosphates are widely used bio-ceramics because they closely mimic the mineral component of bones and teeth in both composition and crystal structure, making them an excellent biocompatible material[40]. This similarity enables calcium phosphates to support protein adsorption, cell adhesion, and subsequent cellular signaling pathways that promote osteoblastic differentiation and matrix mineralization[40]. They are also osteoconductive and form a direct chemical bond with bone tissue, reducing the probability of chronic inflammation leading to fibrous encapsulation[40–42].

While bioactive ceramics, such as the calcium phosphates and bio-glass, are biocompatible and osteoconductive, with excellent corrosion resistance and high compressive strengths[42,43], their intrinsic brittleness and low tensile strength restrict their shaping into complex shapes as well as their use as a single material in load-bearing applications[38]. Additionally, their relatively slow degradation rate may not match the rate of new tissue formation[44]. This limitation has been overcome by integrating bio-ceramics into resorbable polymers, creating composite scaffolds that remain flexible yet possess enhanced mechanical strength and tunable degradation profiles[43,44]. Despite these challenges, their biological affinity with bone tissue makes calcium phosphates a cornerstone material in scaffold design, particularly for bone tissue engineering applications where biological integration is paramount[44].

2.3.2 Polymers

Polymers, formed through the polymerization of monomers, can be engineered to exhibit an extensive range of mechanical properties, degradation profiles, and surface chemistries, making them suitable for both hard and soft tissue requirements[45–47]. They can be broadly divided into natural and synthetic polymers for tissue engineering applications.

2.3.2.1 Natural Polymers

Natural polymers occur naturally in nature and can be extracted from biological material sources and tend to possess biochemical cues that aid cell adhesion, migration, and differentiation[48,49]. They can be categorized into protein polymers and polysaccharide polymers. Although they closely resemble native ECM components, they often exhibit inferior mechanical strength, batch-to-batch variability owing to the inconsistencies in biological sources, and relatively rapid enzymatic degradation when compared to synthetic polymers[49–51]. Hence, for load-bearing applications, natural polymers are either combined with other materials such as ceramics to form composites or undergo chemical modification to increase their strength[51].

2.3.2.1.1 Collagen

Collagen, the most abundant structural protein in the ECM, is widely utilized in tissue engineering, providing mechanical support for cell adhesion and biochemical cues that determine cell fate[50,52]. Collagen, as a protein polymer, exhibits low immunogenicity, excellent biocompatibility, biodegradability by collagenases, and structural resemblance to the native ECM of bones, skin, cartilage, and tendons[51,52]. Its characteristic triple-helical structure, organized fibrillar architecture, and abundance of integrin-binding motifs collectively make collagen an ideal scaffold material, as these structures create a highly supportive environment for cell adhesion, proliferation, and lineage-specific differentiation[48–51,53].

Collagen scaffolds can be fabricated into various forms, including hydrogels, films, sponges, and porous three-dimensional matrices, allowing them to be tailored for specific tissue engineering applications[50,51]. However, collagen's relatively low mechanical strength and susceptibility to rapid enzymatic degradation limit its use as a standalone material in load-bearing environments[51]. Consequently, its mechanical performance and degradation profile often require enhancement

through reinforcement or crosslinking strategies[50]. Despite these limitations, collagen's exceptional biological relevance and its ability to direct cell behavior and tissue remodeling continue to make it one of the most versatile and effective natural polymers for regenerative scaffold design.

2.3.2.1.2 Elastin

Elastin is a key protein polymer component of the ECM that is responsible for imparting elasticity, flexibility, and resilience to tissues, primarily skin, lungs, ligaments, and blood vessels, due to its unique ability to undergo repeated stretching and recoil without permanent deformation[3,54]. Elastin or elastin-derived peptides as a biomaterial in scaffold design closely replicate the elastic properties of the native ECM, particularly in soft tissue applications[55]. Elastin-containing scaffolds facilitate cell adhesion, proliferation, and matrix remodeling while maintaining mechanical stability under dynamic physiological loading, making them valuable components in engineered constructs for elastic tissue regeneration[3,54]. Furthermore, elastin-containing scaffolds can enhance the viscoelastic behavior of engineered tissues, making them particularly valuable in regenerative medicine strategies that require biomimetic mechanical properties[54]. However, the isolating and processing of native elastin at scale faces technical limitations and is often substituted with recombinant elastin-like polypeptides, which still require careful optimization to achieve an appropriate balance of elasticity, mechanical strength, and long-term stability[46].

2.3.2.1.3 Alginate

Alginate, unlike collagen and elastin, is a naturally derived anionic polysaccharide protein polymer extracted primarily from brown seaweed and is often used for hydrogel-based scaffolds due to its excellent biocompatibility, biodegradability, and gelation properties[46,56]. Alginate, in the presence of β-D-mannuronic acid and α-L-guluronic acid residues, undergoes mild gelation to form

hydrogels through ionic crosslinking with divalent cations of calcium; this creates a three-dimensional network that closely resembles the hydrated environment of native ECM[57].

Alginate hydrogels provide a hydrated, highly permeable environment that supports nutrient and waste transport, which supports cell survival, proliferation, and tissue development[56,57]. Furthermore, alginate can be fabricated into hydrogels, beads, porous scaffolds, fibers, and bioinks for 3D bioprinting[56]. While alginate lacks intrinsic cell-adhesive motifs, its bioactivity and mechanical properties can be enhanced through the conjugation of adhesion peptides such as RGD or by blending with proteins and biomaterials including but not limited to gelatin, collagen, and hydroxyapatite[44,56–58]. These modifications can address alginates' poor cell-material interactions while leveraging their tunable mechanical properties, low cytotoxicity, and ability to mimic soft tissues[56].

2.3.2.2 Synthetic Polymers

Synthetic polymers are frequently applied in tissue engineering and regenerative medicine owing to their controllable physicochemical properties, reproducibility, and ease of manufacturing and processing[59]. Unlike natural polymers, synthetic materials can be engineered to achieve specific scaffold structural and mechanical configurations such as pore size, elasticity, degradation rate, and mechanical strength, making them highly adaptable and allowing greater control over the cellular microenvironment[59].

Common synthetic materials used in scaffold fabrication include polylactic acid (PLA), polyglycolic acid (PGLA), polycaprolactone (PCL), polylactic-co-glycolic acid (PLGA), and polyethylene glycol (PEG)[44]. These materials can be fabricated into fibers, films, hydrogels, porous scaffolds, and 3-D printed constructs for use in bone, cartilage, vascular, neural, and skin

tissue engineering. However, since many synthetic polymers lack intrinsic biological recognition sites for cell attachment, they often require surface modification or combination with natural polymers to enhance cellular interactions[44].

2.3.2.2.1 Polylactic acid (PLA)

Polylactic acid is a biodegradable polyester commonly used in tissue engineering due to its great mechanical strength and relatively slow degradation rate[60]. As a polyester, it degrades through hydrolysis into lactic acid, which the human body can safely metabolize.[60]. However, the hydrophobic nature of the material can limit cell adhesion, and an accumulation of the acidic byproduct of degradation, lactic acid, can lead to localized pH reductions, possibly affecting cell viability[60].

2.3.2.2.2 Polylactic-co-glycolic acid (PLGA)

PLGA is a copolymer of lactic acid and glycolic acid engineered to offer tunable degradation through precise ratio control of lactic to glycolic units and mechanical properties for tissue engineering and drug delivery applications, as it degrades more rapidly than PLA[60,61]. It degrades through the hydrolysis of ester linkages, yielding lactic and glycolic acid by-products that naturally enter metabolic pathways, supporting its biocompatibility[62]. Despite its versatility, PLGA produces acidic degradation products and lacks inherent cell recognition sites, requiring peptide functionalization, surface modifications, or blending with natural polymer materials to enhance biological performance[61].

2.3.2.2.3 Polyethylene Glycol (PEG)

PEG is a hydrophilic, biocompatible synthetic polymer with chemical versatility frequently used in hydrogel systems and drug delivery applications[44,61]. Its resistance to protein adsorption

minimizes unwanted cell adhesion, creating an environment where specific biochemical cues can be induced through bioactive peptides in a controlled manner[63]. Its tunable molecular weight and ability to form hydrogels through chemical crosslinking enable the creation of scaffolds with adjustable stiffness, swelling behavior, and degradation profiles[61–63]. However, although PEG provides excellent tunability and cytocompatibility, its inherently bioinert character necessitates additional surface modifications, as unmodified PEG does not actively promote cell adhesion or support tissue formation[61,63].

2.3.3 Metals

Metallic biomaterials, including titanium, stainless steel, and biodegradable magnesium alloys, represent a class of materials that are primarily used in applications requiring high mechanical strength, namely orthopedic and dental implants[13]. Biodegradable metallic biomaterials, such as magnesium alloys, are engineered to provide mechanical support during the early phases of tissue healing while gradually degrading through electrochemical corrosion into biocompatible ions that can be metabolized by the human body or excreted, removing the need for secondary surgical removal[13]. However, challenges such as corrosion control, ion release, and mismatch in mechanical properties with surrounding tissue leading to stress shielding must be carefully considered in the choice of metallic biomaterials[13].

2.4 Scaffold Manufacturing

While the choice of biomaterial is essential for determining a scaffold's biocompatibility, degradation profile and mechanical behavior, the fabrication technique plays an equally critical role as it ultimately defines the scaffold architecture and functional performance. The method used to construct a scaffold governs key parameters including pore size, porosity, interconnectivity, mechanical strength and surface morphology[64]. Conventional techniques ranging from solvent

casting and particulate leaching to freeze drying, electrospinning, gas foaming and thermally induced phase separation each offer distinct advantages in controlling these features and tailoring the scaffold for different tissue requirements[65].

2.4.1 Particulate Leaching

Solvent casting and particulate leaching is a fabrication technique that creates a porous structure by incorporating a temporary porogen, salt, sugar, polyethylene glycol, or paraffin particles, homogeneously dispersed into a polymer solution, casting the mixture into a mold, and then dissolving the porogen to leave behind an interconnected pore structure[65]. The size and volume fraction of the porogen determine the resulting pore size and porosity. It is a simple, low-cost technique suitable for many biodegradable polymers[65,66]. However, its limitation lies in its difficulty in producing interconnected pores, its limited control over complex 3D geometries, and the potential for residual solvent or porogen contamination if washing is incomplete[65].

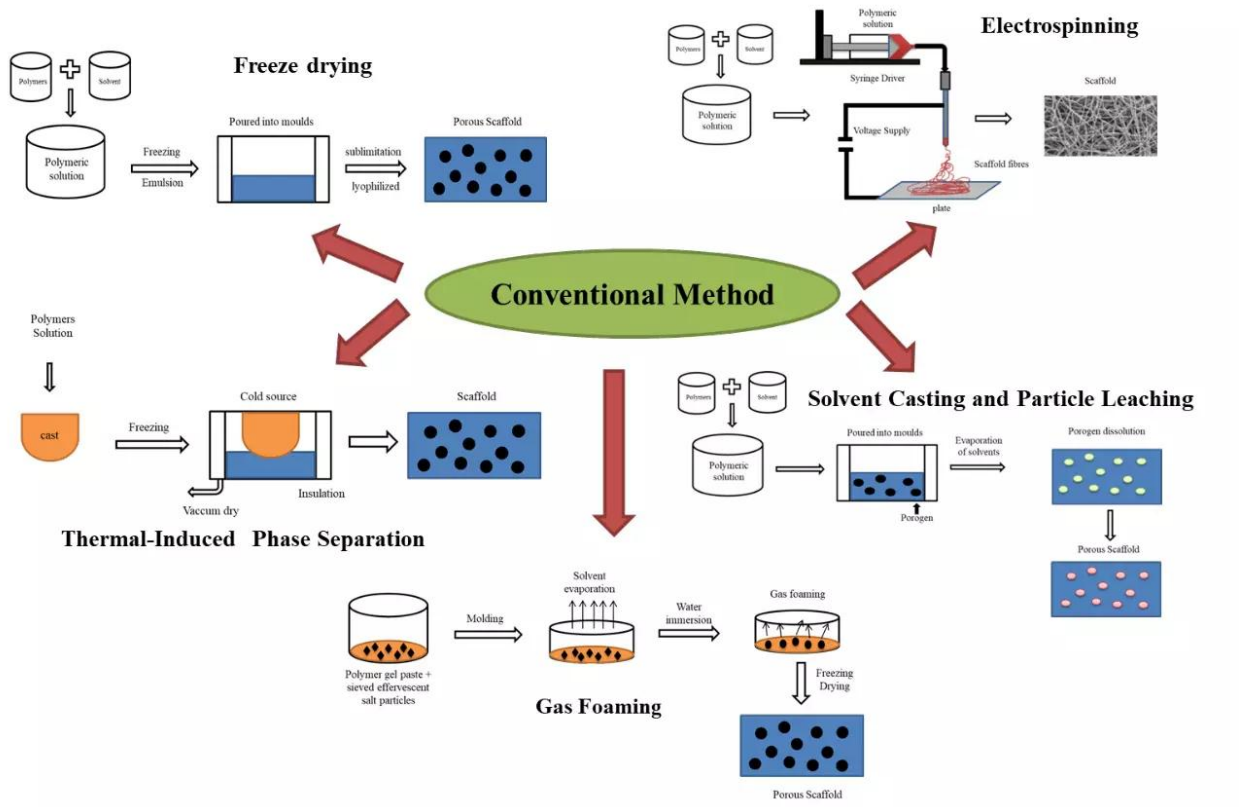

Figure 2.3: Schematic overview of conventional fabrication techniques used to generate porous polymeric scaffolds for tissue engineering applications. The diagram illustrates five widely employed methods—freeze drying, electrospinning, thermal-induced phase separation, solvent casting and particle leaching, and gas foaming—each highlighting the sequential processing steps that govern pore formation, structural morphology, and final scaffold architecture, adapted from[65]

2.4.2 Freeze drying

Freeze drying, or lyophilization, is used to fabricate highly porous, sponge-like structures from hydrophilic polymers and biopolymers such as collagen, gelatin, chitosan, and composite hydrogels[65]. The technique involves freezing a polymer or gel solution under controlled conditions, leading to the formation of solvent crystals that act as a temporary porogen. The frozen solvent is then subsequently sublimated under vacuum, leaving behind a solid interconnected network with pores corresponding to the former crystal spaces[64,65].

The freezing rate, temperature gradient, and solution concentration determine the crystal morphology, pore size, orientation, and connectivity[64]. While this technique produces highly interconnected porous scaffolds in the absence of toxic porogens, there is limited control over pore size uniformity, which depends on the freezing rate and thermal gradients[64]. Additionally, freeze-dried scaffolds tend to have relatively poor mechanical strength and might require post-processing to achieve sufficient strength for lead-bearing applications[64,65].

2.4.3 Electrospinning

Electrospinning is a versatile scaffold fabrication technique used to produce fibrous scaffolds composed of micro- to- nano scale ultrafine polymer fibers by applying a high-voltage electric field to a polymer solution and drawing it into continuous filaments that solidify into a nonwoven fiber mat upon reaching the ground collector[64,65]. Polymers typically utilized include PLA, PLGA, collagen, and gelatin. Electrospinning produces fibrous scaffolds with a high surface area-to-volume ratio and interconnected pore networks formed from the voids between fibers[64]. An advantage of electrospinning is the fine control it allows over fiber diameter, orientation, and composition by adjusting solution properties, processing parameters, and ground collector design[65]. However, electro-spun mats tend to have restricted pore sizes, which hinder deep cell infiltration[66]. It also faces challenges in producing thick 3d constructs without compromising porosity[65,66].

2.4.4 Gas foaming

Gas foaming is a solvent-free scaffold fabrication technique that generates porosity through the expansion of gas bubbles within a polymer matrix, typically PLGA and polycaprolactone (PCL)[64,66]. During processing, the polymer is initially saturated with carbon dioxide under high pressure[65,67]. When the pressure is dropped rapidly, it induces nucleation and growth of gas

bubbles, yielding a network of pores throughout the polymer material[65,67]. Gas foaming can produce scaffolds with high porosity in the absence of cytotoxic porogens, which is advantageous for biological applications[64–67]. However, gas foaming often results in closed or poorly interconnected pores with limited control over pore size distribution and spatial uniformity[66,67]. It also faces challenges in fabricating complex geometries.

2.4.5 Thermal-Induced Phase Separation

Thermally induced Phase Separation is a thermodynamic fabrication technique that uses temperature changes to drive a homogeneous polymer solution to phase-separate into two distinct phases during cooling, creating a uniform porous structure[65]. The process involves dissolving a polymer at elevated temperatures to form a clear homogeneous solution. When the temperature is reduced, it induces separation into a polymer-rich and polymer-poor phase[65]. Subsequently, it is frozen through crystallization, and the solvent is extracted, leaving behind a highly porous scaffold whose morphology depends on the cooling rate, polymer concentration, and solvent choice[65]. While the process offers the advantage of producing interconnected pores with tunable microporous structures without the use of cytotoxic porogens, it is relatively slow and struggles to achieve precise control in complex 3D geometries[65].

2.5 Crosslinking Techniques

While fabrication techniques define the overall architecture and morphology of a scaffold, many methods, including freeze-drying and gas foaming, often produce constructs with insufficient mechanical strength for load-bearing applications, necessitating post-processing. Additionally, type 1 collagen that is reconstituted into scaffolds lacks the crosslinks present in native ECM, resulting in scaffolds with poor mechanical resilience, poor resistance to enzymatic degradation, and limited structural stability. Crosslinking is a post-processing method that reinforces polymer

networks by forming covalent or physical bonds between polymer chains[19,68,69]. These methods are broadly categorized into three classes based on their underlying mechanism of action: chemical crosslinking, which forms covalent bonds between amino acid side chains; physical crosslinking, which uses energy to induce radical-mediated bond formation; and enzymatic or biological crosslinking, where enzymes are used as catalysts for bond formation[70].

Chemical crosslinking methodologies can be further categorized based on the underlying chemical mechanisms of action. These are classified into aldehydes, isocyanates, carbodiimides, and epoxides[71]. Aldehydes, particularly Glutaraldehyde (GA), produce strong covalent bonding and structural reinforcement[71,72]. However, literature reports its cytotoxic potential and limited control over long-term degradation[70–72]. Isocyanates, such as Hexamethylene Diisocyanate (HMDI), form strong covalent bonds through the formation of urethane linkages by reacting with nucleophilic groups, primarily the hydroxyl, amine, and carboxyl groups on polymer chains[71]. While more cytocompatible than GA, studies report limited degradation resistance and the potential to release toxic intermediates, leading to foreign body responses, which raises biocompatibility concerns[71].

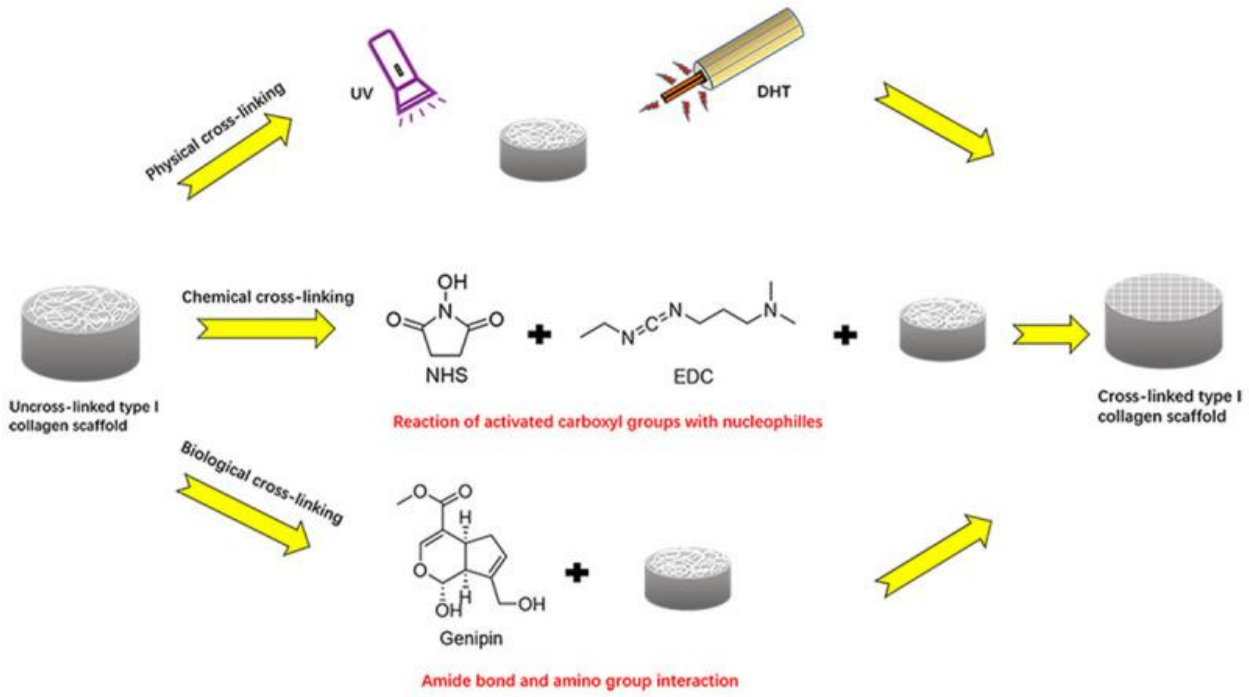

Figure 2.4: Schematic representation of three major cross-linking strategies used to stabilize type I collagen scaffolds. Physical cross-linking methods include UV irradiation and dehydrothermal treatment. Chemical cross-linking involves carbodiimide chemistry (EDC/NHS) to activate carboxyl groups to form covalent linkages within the collagen network. Biological cross-linking uses naturally derived agents such as genipin to generate stable amide bonds. Adapted from[70]

The most commonly used crosslinker for biomedical research, primarily protein conjugation, is 1-ethyl-3-(3-dimethylaminopropyl) carbodiimide hydrochloride (EDC) and N-Hydroxysuccinimide (NHS), as it creates zero-length amide bonds[70–73]. Unlike other chemical crosslinkers, which introduce additional chemical compounds, EDC activates a carboxylate group in the polymer chains to form an unstable reactive O-acylisourea intermediate, which is prone to rapid hydrolysis[71]. NHS is added to stabilize the intermediate by converting it into an NHS ester, which then reacts with a primary amine to form a covalent amine bond[70,71]. Because the by-products are water-soluble and easily removed, EDC/NHS crosslinking is considered highly cyto-compatible[71–73]. The resulting amide bonds enhance mechanical strength and reduce degradation by stabilizing

hydrolysis-susceptible sites, while still allowing predictable long-term breakdown of the scaffold[71].

Biological or enzymatic crosslinking tends to mimic in vivo ECM crosslinking, where enzymes such as transglutaminases generate specific covalent bonds that govern collagen fiber mechanics[70,72]. Transglutaminases catalyze the formation of ε-(γ-glutamyl) lysine isopeptide bonds between glutamine and lysine residues, forming stable crosslinks that resist proteolysis and thermal denaturation[71,72]. When applied to type I collagen gels, microbial transglutaminase significantly increases denaturation temperature, enhances mechanical properties, and reduces matrix swelling[70,71]. Compared with non-specific chemical crosslinkers, TG-mediated crosslinking offers high specificity and minimal toxic residues, making it suitable for cell-culture scaffolds, but with higher cost and greater sensitivity to processing conditions than traditional chemical or physical methods[70].

Physical crosslinking utilizes energy input to induce covalent bonds and network rearrangement[70,71]. Ultraviolet (UV) irradiation induces the formation of covalent bonds between polymer chains through photoactivation, which photosensitizers can enhance to increase network stiffness[70]. In collagen systems, UV irradiation can be used to stabilize films and hydrogels with the ability to sterilize the scaffold surfaces simultaneously[71]. However, UV irradiation is limited by its shallow penetrating depth, making it suitable for thin films[71].

In contrast, high-energy ionizing radiation such as gamma irradiation is more commonly used for terminal sterilization of medical devices and collagen-based biomaterials due to its high penetrating depth[72]. Its ability to induce radical-mediated bond formation in both water and polymer backbones makes it a suitable physical crosslinker[71]. However, the interplay between

crosslinking and sterilization can induce chain damage in the polymer chain[74]. In collagen, low-to-medium gamma dosage can increase crosslinking, while high dosages can cause denaturation of collagen's triple-helix structure and chain scissions[74,75]. Hence, physical methods of crosslinking such as UV and gamma irradiation are often used in complement with chemical and enzymatic crosslinking to avoid detrimental structural changes to the polymer[70,71].

2.6 Sterilization techniques

Sterilization is the terminal step in the fabrication of implantable biomaterials that aims to eliminate all microbial contaminants and agents to prevent infection and adverse immune response post-implantation. However, many sterilization techniques can alter the scaffolds' physicochemical and biological properties, including morphology, mechanical integrity, and cell-material interactions, and are quite common in protein-based biomaterial scaffolds[76,77]. Additionally, some sterilization techniques can induce cytotoxic effects in the biomaterials[78]. Common sterilization techniques include physical heat-based or ionizing methods such as autoclaving, gamma and X-ray irradiation, and chemical approaches such as ethylene oxide treatment, which have been utilized successfully in terminal sterilization of collagen-based scaffolds.[78,79]. Each method presents distinct advantages and limitations in terms of penetration depth, effectiveness, and potential material degradation. Hence, the choice of technique depends on the scaffold composition and intended application to modulate the biomaterials' properties to fit. Hence, there is no standard method of sterilization for biomaterials[79].

Gamma Irradiation has two mechanisms of action that break down the nucleic acid of microbial cells[79]. The direct approach involves the use of high-energy photons on the material to target the genetic material of the microbial cells [80]. The energy from the generated free radicals cleaves the phosphodiester backbone of the DNA strands, which permanently alters the cells' ability to

replicate[81]. The indirect approach is an effect of the radiolysis of water, as cells are mostly composed of water. The gamma rays ionize intracellular water molecules into unstable free radicals that diffuse through cells and chemically react with nucleic acids and the cellular membrane, damaging them; for polymer-based scaffolds, including collagen-based biomaterial scaffolds, gamma irradiation has shown evidence of sterilization and crosslinking, increasing tensile strength and stiffness at appropriate dosages[79,81]. However, collagen is particularly sensitive to ionizing radiation, and a moderate sterilization dosage of 25 KGy can cleave peptide backbones, induce chain scission, and denature the triple helix structure, with several studies reporting severe damage to collagen molecules attributed to gamma irradiation[74]. These structural changes can alter long-term mechanical behavior and degradation profiles, meaning that gamma dose and matrix formulation must be carefully optimized.

X-ray irradiation is a high-energy form of ionizing electromagnetic radiation used in the terminal sterilization of food, medical devices, and polymeric materials due to its deep penetration, low thermal load, and short treatment time[79]. As an ionizing source, it generates high-energy photons that disrupt microbial DNA and cellular structure, ensuring sterility in the absence of moisture at temperature levels that do not induce damage to polymeric systems[82]. Ionizing radiation can generate free radicals within polymer matrices, leading to chain scission and/or secondary crosslinking, depending on the polymer chemistry, irradiation dose, and surrounding environment[78,82]. While X-ray exposure is well-characterized in the context of medical imaging and radiotherapy—particularly regarding its effects on cellular behavior—the impact of such ionizing radiation on the extracellular matrix and biomaterial scaffolds remains comparatively underexplored[82].

In natural polymer systems such as collagen, sterilization-level X-ray doses (~12 KGy) can induce both structural and chemical modifications that manifest as reduced tensile strength, altered viscoelastic behavior, and shifts in degradation kinetics[83]. These effects are often magnified in heterogeneous biopolymers, which are more susceptible to radiation-induced denaturation, fragmentation, or secondary crosslinking[84,85]. Moreover, batch-to-batch variability and differences in post-processing techniques can produce inconsistent irradiation responses, complicating efforts to maintain predictable mechanical performance across scaffold constructs[79]. Consequently, a detailed understanding of polymer-specific radiation responses is essential for designing biomaterials that preserve structural integrity following terminal sterilization.

2.7 Characterization

The characterization of collagen- based scaffolds is required to understand how the composition, structure, and processing conditions influence the scaffolds' performance. As the collagen matrix can affect cell adhesion, spreading, proliferation, and lineage determination, characterization focuses on collagen hierarchical architecture, crosslinking-dependent stability, degradation kinetics, and cell-matrix interactions[7,8,86]. Hence, across the literature, studies characterize collagen scaffolds using a combination of morphological, mechanical, thermal, chemical, and degradation-based analyses to connect scaffold architecture with biological function[77,85–91].

Structural and/or morphological characterization evaluates the pore architecture, fiber arrangements, and pore interconnectivity, which are essential as they regulate nutrient diffusion, cell infiltration, and vascularization[92]. Some common characterization techniques include scanning electron microscopy (SEM), which visualizes the scaffold's microstructure; atomic force microscopy (AFM), which is used for micro- and nanoscale fibrillar organization, imaging, and force characterization; and X-ray diffraction (XRD), which is used to assess crystallinity[53,93].

Thermochemical analysis is used to verify collagen integrity, crosslinking degree, thermal stability, and alteration induced by the processing conditions[86,90,92]. Fourier-transform infrared spectroscopy (FTIR) confirms collagen identity and the preservation of its triple-helical structure, and it is also used to detect chemical modifications induced by thermal aging, crosslinking, or the sterilization process[17,91,94]. Differential scanning calorimetry measures the denaturation temperature and thermal transition points[86,92]. Together, these analyses determine whether the scaffold retains the molecular properties associated with native ECM collagen.

Mechanical characterization ensures that the scaffolds can withstand loading and implantation by possessing adequate strength, stiffness, and elasticity for their intended tissue environment[16,69,86]. Tensile, compressive, and rheological testing are used to quantify the elastic moduli (E), ultimate tensile strength (UTS), strain at failure, and viscoelastic behavior under physiologically relevant conditions. Processing conditions strongly influence the mechanical performance of polymeric scaffolds[16]. Literature reports that free-drying rate, crosslinking, and sterilization significantly alter mechanical properties[16,92,95]. This is relevant in collagen-based systems as it highlights collagen sensitivity to fabrication conditions.

In addition to structural and mechanical tests, other studies such as enzymatic degradation and biocompatibility are considered, as these properties are related to in vivo performance. Biodegradation studies assess collagen stability in the presence of enzymes under physiological conditions[88,92]. While crosslinking slows degradation, conventional chemical crosslinkers tend to leave cytotoxic residue or significantly alter mechanical properties[88]. A recent study showed that incorporating L-serine into collagen scaffolds modulated the degradation kinetics in the absence of chemical crosslinking in mouse models[96]. Additionally, cell proliferation assays, cytotoxicity testing, and differentiation assays assess cell viability and fate on the scaffold and how the

scaffold's properties are modulated[86]. This demonstrates how biochemical modification can tune degradation kinetics and cell viability while maintaining biocompatibility.

In summary, current research demonstrates that collagen-based scaffolds are promising biomaterials for tissue engineering due to their biocompatibility, bioactivity, and structural similarity to native ECM. However, the extent of their application remains constrained by limitations in mechanical strength, thermal stability, and resistance to enzymatic degradation, properties that are influenced by source materials, fabrication method, crosslinking technique, and sterilization treatment. Collectively, this review shows that scaffold design requires a balance between structural stability and biological performance supported through comprehensive integrated characterization encompassing morphology, mechanical behavior, chemical structure, and degradation kinetics.

Chapter 3: Materials and Methods

3.1 Collagen Slurry Preparation

1 g of Type I collagen powder, sourced from bovine Achilles tendon (Sigma-Aldrich Co. Ltd., UK, Cat. #C9879), was dissolved in 100 mL of 0.05 M acetic acid (Sigma-Aldrich Co. Ltd.) and stored at 4°C for 8–24 hours to rehydrate. The solution was homogenized on ice to form a slurry, then degassed under vacuum to eliminate air bubbles. For the composite scaffold, hydroxyapatite and elastin were added to the slurry in predetermined ratios and homogenized on ice. The solution was then degassed to remove air bubbles. The final solution was stored in 50 mL conical tubes in a refrigerator at 4°C to await further use.

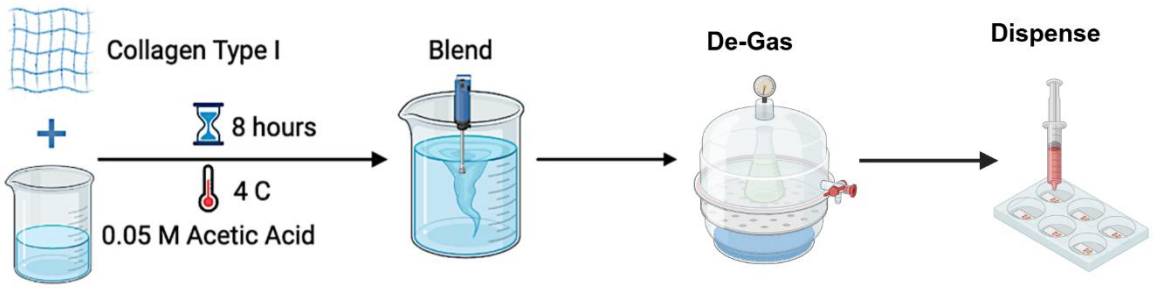

Figure 3.1: Schematic representation of collagen powder swelling and homogenization process.

3.2 2D Scaffold Preparation

Collagen scaffolds were prepared by solution casting to produce two-dimensional(2D) films. Using a syringe, 1.5 mL of the solution was dispensed into each well of a non-TC-treated 6-well plate and left to dry overnight in a fume hood, under ambient conditions, resulting in 1% by weight collagen 2d scaffolds. After 48 hours, the dried films were carefully detached from the well plates, packaged, and stored in a dry state at 25 °C until further use.

3.3 X-ray Sterilization

Scaffolds were sterilized using X-ray irradiation at a dose of 25 kGy under ambient conditions. Samples were sealed in sterile packaging before irradiation. Control (non-irradiated) scaffolds were maintained for comparison.

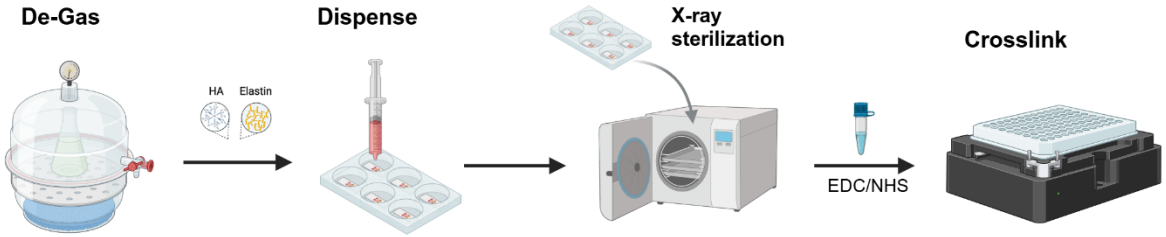

Figure 3.2: Schematic representation of the sterilization and crosslinking of the collagen-based 2D scaffolds.

3.4 Crosslinking

Chemical crosslinking was performed using an EDC–NHS system. A crosslinking solution containing 1-ethyl-3-(3-dimethylaminopropyl) carbodiimide hydrochloride (EDC, Sigma-Aldrich Co. Ltd., UK, Cat.# 161462) and N-hydroxysuccinimide (NHS, Sigma-Aldrich Co. Ltd., UK, Cat.# 6066-82-6) was prepared at a molar ratio of 5:2:1 (EDC: NHS: collagen). For every 1 mg of collagen, this corresponded to 1.15 mg EDC and 0.276 mg NHS dissolved in 80% ethanol. Scaffolds were immersed in the crosslinking solution and reacted for 3 h at room temperature under agitation using an orbital shaker set to 200 rpm. Following crosslinking, scaffolds were washed twice in sterile phosphate-buffered saline (PBS Sigma-Aldrich Co. Ltd.), with each wash lasting 15 min to remove residual reagents. An additional wash with Milli-Q water was performed

to remove residual salts from the PBS. Scaffolds were then left to dry overnight at room temperature and subsequently stored in a dry state at 25°C until further use. Control samples (non-crosslinked) were maintained for comparison.

3.5 Experimental groups

To systematically evaluate the effects of composition, irradiation, and crosslinking on scaffold performance, a series of experimental groups were defined. Scaffolds were first categorized based on material composition into collagen-only scaffolds and composite scaffolds.

Within each composition group, samples were further divided based on exposure to X-ray irradiation, resulting in irradiated and non-irradiated conditions. Each of these groups was subsequently subdivided based on crosslinking treatment, yielding crosslinked and non-crosslinked scaffolds.

This hierarchical design resulted in four primary conditions for each scaffold type: (i) non-irradiated, non-crosslinked; (ii) non-irradiated, crosslinked; (iii) irradiated, non-crosslinked; and (iv) irradiated, crosslinked.

All scaffold groups were subjected to the same set of characterization techniques, including thermal analysis (DSC), mechanical testing (tensile and rheological measurements), Spectroscopy (FTIR), and enzymatic degradation using collagenase. This approach enabled direct comparison of the individual and combined effects of irradiation and crosslinking across different scaffold compositions.

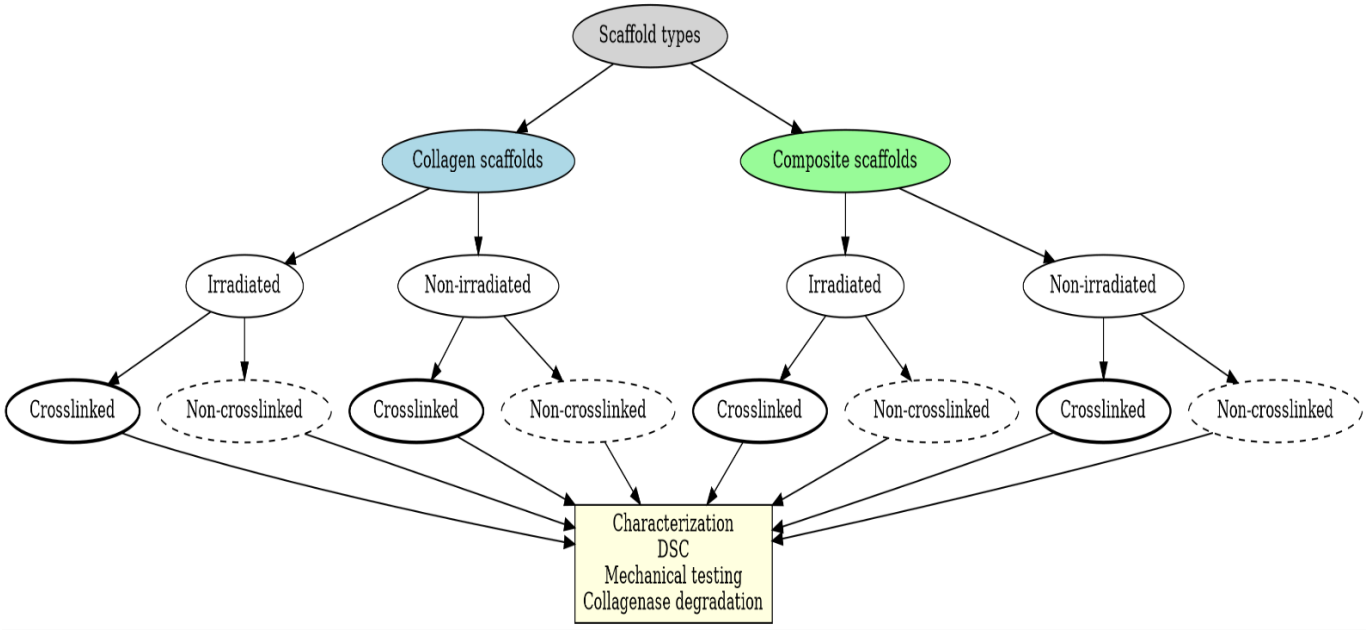

Figure 3.3: Hierarchical organization of scaffold groups and experimental conditions used in this study. Scaffold types are categorized into collagen and composite formulations, each further subdivided into irradiated and non-irradiated variants. Within each irradiation condition, scaffolds are classified as crosslinked or non-crosslinked, forming the full matrix of experimental groups subjected to downstream characterization. All scaffold variants undergo thermomechanical testing, secondary structure analysis, and collagenase degradation analysis to evaluate thermal stability, structural integrity, and enzymatic susceptibility.

3.6 Differential Scanning Calorimetry

Thermal properties were analyzed using differential scanning calorimetry (DSC 2500, TA Instruments) to evaluate the thermal stability of the collagen component of the collagen-only and composite scaffolds as a method to quantify the effects of EDC/NHS crosslinking and X-ray sterilization on collagen denaturation behavior. DSC provides a measure of the thermal transition temperature (T_d) associated with the disruption of collagen's triple helical structure.

Samples (5- 10 mg) were hermetically sealed in aluminum pans and heated from 25°C to 100°C at a rate of 5°C/min under a nitrogen atmosphere with a flow rate of 330ml/min. The denaturing temperature (T_d) was determined from the peak of the endothermic transition. The onset, peak, and

completion temperatures reflect the degree of hydrogen bond stability within the collagen network. At the same time, the enthalpy of denaturation estimates the amount of energy required to unravel the triple helical structure of collagen.

3.7 Rheological testing

Mechanical properties of the 2D collagen scaffolds were characterized using a Discovery Hybrid Rheometer (DHR-3, TA Instruments) equipped with a tensile testing fixture, including elastic modulus (E), Ultimate tensile strength (UTS), and strain at fracture. Rectangular samples of approximate cross sections of 10mm by 40mm, with thickness ranging from 0.03 to 0.08 mm, were mounted securely under a standardized gauge length, and controlled axial tensile tests were performed at a constant strain rate to determine the engineering stress under strain.

Each specimen was first subjected to a small preload of 0.01 N to ensure proper alignment and eliminate slack before testing. After pre-stretching, the crosshead was driven at a constant rate of 0.1mm/s until the sample reached mechanical failure. The resulting load–displacement data were used to compute engineering stress and strain.

Engineering stress (σ) was determined by dividing the measured force (F) by the initial cross-sectional area (A_0, calculated as width × thickness):

$$\sigma = \frac{F}{A_0}$$

Engineering strain (ε) was calculated by the change in gauge length (Δl) divided by the original gauge length (l_0):

$$\varepsilon = \frac{\Delta l}{l_0}$$

The linear elastic region of the stress-strain curves was used to calculate the elastic modulus. The maximum stress sustained before failure was recorded as the UTS, and the strain percentage at that point was recorded as the strain at fracture. Sample geometry and strain rate were standardized across all tests to ensure reproducibility and to isolate the effects of crosslinking and sterilization on tensile performance. All scaffolds were 2D dry films tested under quasi-static uniaxial tension, and all stress–strain data were baseline-corrected before analysis, with tensile values reported as positive.

3.8 Fourier Transform Infrared Spectroscopy (FTIR)

ATR-FTIR (Attenuated Total Reflectance Fourier Transform Infrared, PMA50, Bruker) spectroscopy was performed on all samples (collagen only and composite scaffold, irradiated and non-irradiated, and crosslinked and un-crosslinked) to verify the chemical composition of the scaffolds and assess the molecular alterations introduced by EDC/NHS crosslinking and X-ray sterilization. Spectra were collected using an ATR (Attenuated Total Reflectance)-FTIR spectrometer with classification performed on the Opus 7.5 software, over a range of 4000 - 400 cm^{-1} with a resolution of 4 cm^{-1}. Each spectrum was averaged over 64 scans. As all the components were homogenized during fabrication, the surface chemistry approximated by the ATR-FTIR probes is assumed to reflect the bulk material.

Amide A, I, II, and III bands were used as indicators of collagen's secondary structure. Amide I (C=O stretching) and amide II (N-H bending/ C-N stretching vibrations) were selected as primary

markers for detecting the structural shifts associated with crosslinking and sterilization[17]. Amide II serves as a reference band as it is less susceptible to processing conditions-induced changes[17].

Elastin was assessed through the CH_2/CH_3 deformation band near 1440-1460 cm^{-1}. Because this region overlaps with a carbonate substitution in hydroxyapatite, this band was interpreted as a composite signal from both materials. Hydroxyapatite was identified through the v_1, v_3, and v_4 phosphate vibrations[97]. These mineral-phase markers were selected because they can be detected while embedded in an organ matrix.

3.9 Collagenase degradation

Enzymatic degradation of 2D collagen scaffolds was assessed using collagenase derived from Clostridium histolyticum. Collagenase was dissolved in a Tris and Calcium chloride $CaCl_2$ buffer solution. Scaffolds (initial dry weight: 3–10 mg) were pre-weighed and placed in 1.5 mL microcentrifuge tubes. Samples were incubated in collagenase solution at a concentration of 30U/mL in the presence of CO_2[98] . Degradation was evaluated over multiple time points across 5 days.

Control samples were incubated in Tris/HCl buffer supplemented with 5mM $CaCl_2$ under identical conditions. At each time point, samples were removed from the incubator, and 100 µl of 0.5 M ethylenediaminetetraacetic acid (EDTA, Invitrogen, USA, Cat.# 15575-038) was added to cleave the calcium ions and stop enzymatic activity[98,99] . Tubes were then placed on ice for 10 min, followed by centrifugation at 12,000 rpm for 10 min. The supernatant was carefully aspirated, and the samples were washed with Milli-Q water and agitated on an orbital shaker at 200 rpm for 5 min on ice. Samples were centrifuged again at 12,000 rpm for 10 min, and the washing step was repeated once more.

After the final wash and aspiration of the supernatant, the remaining material was dried in a fume hood for 7 days. The dry mass was recorded, and the percentage of mass remaining was calculated relative to the initial scaffold weight.

$$\text{Mass remaining}(\%) = \frac{m_t - m_o}{m_o} \text{ x } 100$$

The half-life was analyzed through an exponential one-phase decay using a pseudo-first-order kinetic model where the rate of degradation is directly proportional to the final amount of intact collagen.

$$Y(t) = 100e^{-Kt}$$

As collagenase derived from Clostridium histolyticum is highly specific to collagen degradation, mass loss degradation in the composite scaffolds was attributed to collagen. The percentage of collagen degradation in the composite was normalized by the ratio of collagen to the other components in the scaffold.

$$Y(t) = 50 + 50e^{-Kt}$$

3.10 Statistical analysis

All experiments were conducted with a minimum of three independent replicates unless otherwise specified. Statistical analyses were performed using GraphPad Prism. Comparisons between experimental groups were carried out using analysis of variance (ANOVA), followed by appropriate poc hoc tests. A significance level of $p < 0.05$ was used for all analyses.

Chapter 4: Results

4.1 Molecular Characterization

FTIR was employed to characterize the molecular composition and secondary structure of collagen/hydroxyapatite/elastin composite scaffolds across 4 processing conditions, with collagen-only scaffolds as a control. The spectra for the collagen-based scaffolds and composite scaffolds are presented separately in Figure 4.1 and Figure 4.2, respectively, with each condition stacked for visual comparison. Across all spectra, the major amide bands characteristic of collagen were observed, including the Amide I, Amide II, and Amide III regions, indicating the preservation of the protein backbone in all scaffold conditions. Characteristic bands confirmed the presence of collagen and other individual components in the heterogeneous scaffold. At the same time, shifts in peak position provided evidence of structural modification induced by EDC/NHS crosslinking and X-ray irradiation.

For the collagen scaffold group, the spectra showed Amide I band (C=O stretching vibration, 1630 cm^{-1} – 1660 cm^{-1}), Amide II band (N-H bending/ C-N stretching vibrations, 1540 – 1560 cm^{-1}), Amide III band (C-N stretching/ N-H bending vibrations, 1220 - 1270 cm^{-1}), the C=O stretch (~1772 cm^{-1}) and the CH_2 bending across the un-crosslinked and crosslinked conditions.

The non-irradiated un-crosslinked sample exhibited the characteristic bands associated with native collagen, including the Amide I band (~1635 cm-1) correlating to the C=O stretching of the triple helix, the Amide II band (~1540 cm-1) reflecting the C-N stretching and N-H bending vibrations, and the Amide III band (~1235 cm^{-1}). The CH_2 bending band (~1450 cm^{-1}) was also present, indicating intact collagen side chains. Together these features confirm that the un-crosslinked, non-irradiated collagen maintained native triple helix structure.

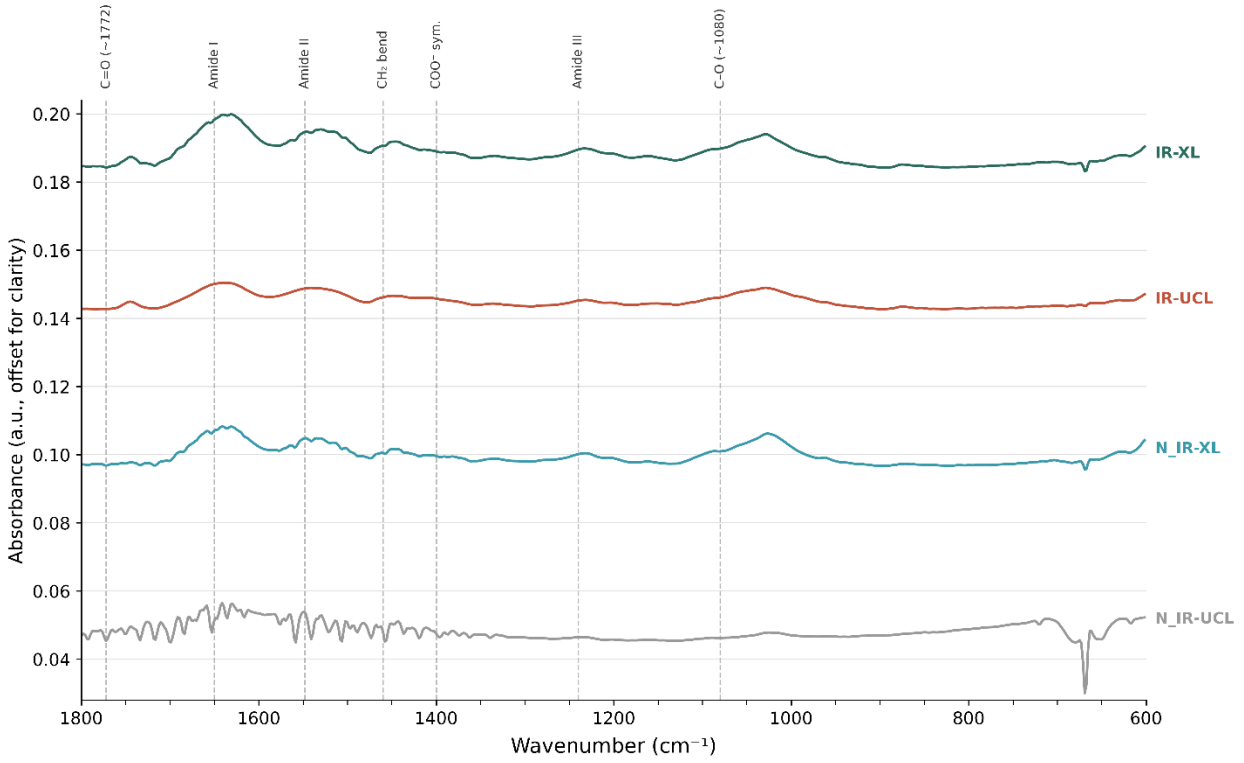

Figure 4.1: FTIR spectra of collagen-only scaffolds in the fingerprint region (1800–600 cm^{-1}). Normalized absorbance spectra are shown for non-irradiated un-crosslinked (N_IR-UCL), non-irradiated crosslinked (N_IR-XL), irradiated un-crosslinked (IR-UCL), and irradiated crosslinked (IR-XL) collagen scaffolds. Key collagen vibrational bands are indicated, including the C=O stretch (~1772 cm^{-1}), Amide I, Amide II, CH_2 bending, COO symmetric stretch, Amide III, and C–O (~1080 cm^{-1}). Crosslinking produced minor shifts in the amide bands, consistent with increased molecular packing. At the same time, sterilization resulted in pronounced downshifts and reduced Amide III intensity, indicating partial denaturation of the collagen triple helix.

The Amide I band was observed at approximately 1641 cm^{-1} in the non-irradiated crosslinked scaffold, 1639 cm^{-1} in the sterile un-crosslinked scaffold, and 1631 cm^{-1} in the sterile crosslinked scaffold. The Amide II band was located at approximately 1545- 1547 cm-1 across the non-irradiated collagen conditions and approximately 1532– 1535 cm-1 for the irradiated collagen groups, while the Amide III band remained visible at approximately 1235- 1245 cm^{-1} across all collagen conditions. Minor shifts in peak position and changes in band intensity were observed between groups, particularly in the sterilized and crosslinked scaffolds.

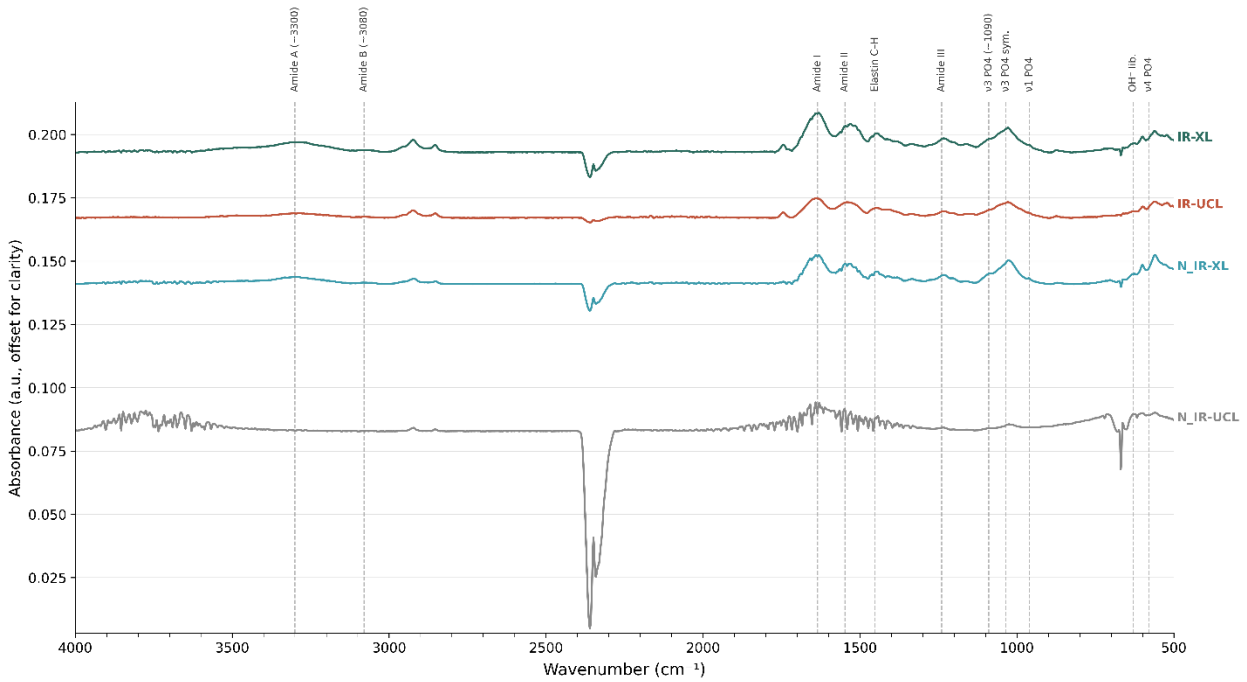

Figure 4.2: ATR FTIR spectra of collagen–hydroxyapatite–elastin composite scaffolds under four fabrication condition: non-irradiated un-crosslinked (N_IR-UCL), non-irradiated crosslinked (N_IR-XL), irradiated un-crosslinked (IR-UCL), and irradiated crosslinked (IR-XL) composite scaffolds. Spectra display characteristic protein bands (Amide A ~3286–3288 cm^{-1}, Amide I 1631–1641 cm^{-1}, Amide II 1529–1549 cm^{-1}, Amide III 1232 cm^{-1}), elastin-associated C–H deformation (1444–1448 cm^{-1}), and hydroxyapatite phosphate modes (ν_3 PO_4^{3-} at 1024–1028 and 1072–1090 cm^{-1}; ν_1 PO_4^{3-} at 960–978 cm^{-1}; ν_4 PO_4^{3-} at 560 and 600 cm^{-1}) and the OH^- liberation band (625–635 cm^{-1}). The persistence of ν_3 and ν_4 doublets and the OH^- band confirms the presence of crystalline hydroxyapatite across all conditions.

For the composite scaffold group, the FTIR spectra also showed the characteristic collagen-related amide bands, along with additional features associated with the composite phase. The spectra were stacked to highlight differences among the eight conditions, and the main peak regions remained detectable across all samples. The Amide I band appeared at approximately 1631 cm^{-1} – 1641 cm^{-1}, the Amide II band at approximately 1529 – 1549 cm^{-1}, and the Amide III band remained at ~1232 cm^{-1} across all conditions. In addition, elastin-associated C–H deformation band (1444–1448 cm^{-1}), hydroxyapatite phosphate modes (ν_3 PO_4^{3-} at 1024–1028 and 1072–1090 cm^{-1}; ν_1 PO_4^{3-} at 960–978 cm^{-1}; ν_4 PO_4^{3-} at 560 and 600 cm^{-1}) and the OH^- liberation band (625–635 cm^{-1}), were

observed in the composite samples, reflecting the presence of the inorganic or second-phase component.

As elastin is a protein polymer like collagen, it does not show fully unique FTIR bands as they overlap mostly with that of collagen[100]. However, a distinct band at 1444 – 1448 cm^{-1} was observed across all composite conditions. This band is consistent with CH_2/CH_3 deformation modes of valine and alanine residues, which are abundant in elastin.

Hydroxyapatite was confirmed in all composite scaffold conditions through the presence of its characteristic phosphate and hydroxyl vibrational modes[101]. The ν_3 PO_4^{3-} stretching doublet (1020 – 1090 cm^{-1})[97,101] was present across all samples, with its lower component (1024 – 1028 cm^{-1})[97,101] remained within range while its upper component shifted from 1089 cm^{-1} in the non-irradiated un-crosslinked scaffold to ~1072 cm^{-1} in the other 3 conditions.

The ν_4 PO_4^{3-} bending doublet at ~560 and ~600 cm^{-1} was also present in all groups, further supporting hydroxyapatite crystallinity[97]. The OH^- liberation band, appearing between 624 - 634 $cm^{-1,}$ confirmed the presence of stoichiometric hydroxyapatite with preserved hydroxyl channels across all composite conditions[101]. Lastly, the ν_1 PO_4^{3-} symmetric stretch shifted from 960 cm^{-1} in the non-irradiated un-crosslinked scaffold to 977 cm^{-1} across the other composite scaffold conditions, exceeding the typical hydroxyapatite range[97,101].

Across both material types, sterilization and crosslinking produced condition-dependent changes in the FTIR profiles. In the un-crosslinked scaffolds (N_IR-UCL and IR-UCL), sterilization shifted the Amide I band by ~2 cm^{-1} from (1641 – 1639 cm^{-1} and the amide II band from 1548 cm^{-1} to 1541 cm^{-1}. Crosslinking of the sterilized scaffold produced the largest wavelength shifts in the spectra (Amide I: ~10 cm-1; Amide II: ~17 cm^{-1}). These differences suggest that scaffold

processing influenced the molecular environment of the collagen matrix, although the overall FTIR profiles remained consistent with the presence of collagen in all groups.

4.2 Thermal Property Characterization

Differential scanning calorimetry was used to evaluate the thermal stability of wet collagen-based scaffolds under eight experimental conditions defined by material type (collagen only and composite), sterility (irradiated and non-irradiated), and crosslinking (crosslinked and un-crosslinked), with n = 3 per group. For all groups, DSC thermograms displayed a characteristic endothermic transition corresponding to collagen triple helix denaturation, from which the onset temperature, denaturing temperature (T_d), and denaturation enthalpy (ΔH) were extracted Figure 4.3. The distribution of Td values is shown in the box-and-whisker plot in Figure 4.4, which displays the median, interquartile range, and full data range for each scaffold condition. A two-way ANOVA was performed for statistical analysis.

For collagen-only scaffolds (Figure 4.3a), the denaturation peak was centered at approximately 59.21 °C for the non-irradiated un-crosslinked condition, 79.89 °C for the non-irradiated crosslinked condition, 39.68 °C for the irradiated un-crosslinked condition, and 75.77 °C for the irradiated crosslinked condition. For composite scaffolds (Figure 4.3b), corresponding peaks occurred at approximately 59.53 °C, 71.10 °C, 50.27 °C, and 56.16 °C for the four composite conditions. These representative thermograms illustrate the shift in denaturation temperature and any broadening or narrowing of the transition peak that accompany changes in processing conditions.

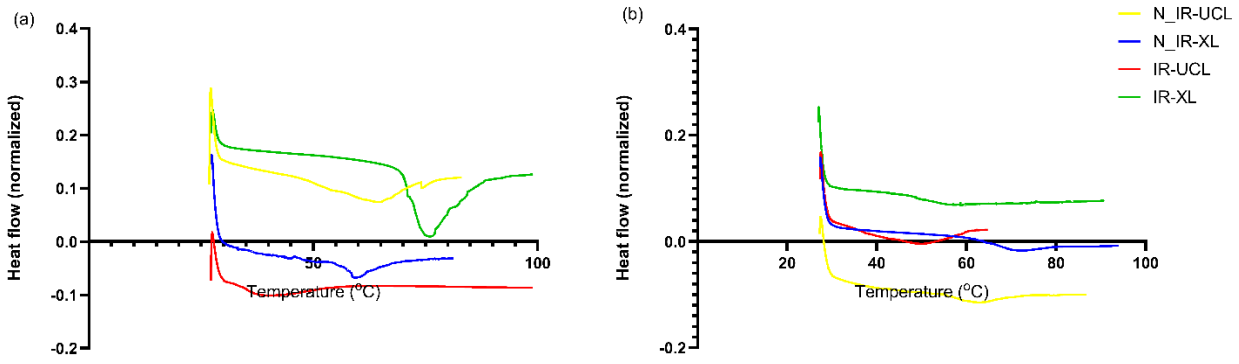

Figure 4.3: DSC Thermograms for the collagen and composite scaffold across the 4 processing conditions. (a) Thermograms for collagen-only film scaffolds processed under four conditions: N_IR-UCL (non-irradiated, un-crosslinked; yellow), N_IR-XL (non-irradiated, crosslinked; blue), IR-UCL (irradiated, un-crosslinked; red), and IR-XL (irradiated, crosslinked; green). Curves illustrate the characteristic endothermic transition associated with collagen denaturation and highlight shifts in thermal stability as a function of irradiation and crosslinking. (b) Corresponding DSC thermograms for composite scaffolds under the same four processing conditions, plotted using the identical color scheme and abbreviations.

When Td values were compared across the row factor (processing conditions), clear differences were observed among the four levels (e.g., non-irradiated un-crosslinked, non-irradiated crosslinked, irradiated un-crosslinked, irradiated crosslinked). The two-way repeated-measures ANOVA showed that the row factor accounted for most of the total variation in T_d (78.4%), with a highly significant effect on denaturing temperature ($p = 0.0004$). This indicates that processing conditions strongly influenced thermal stability.

The column factor, corresponding to scaffold material type (collagen-only vs composite), also had a statistically significant main effect on Td. The column factor contributed ~1.902 % of the total variation, with a p-value of 0.0449, indicating a modest but significant difference between material types. On average, the collagen-only scaffolds exhibited a higher Td (63.52 °C) than the composite scaffolds (60.12 °C), with a mean difference of 3.41 °C.

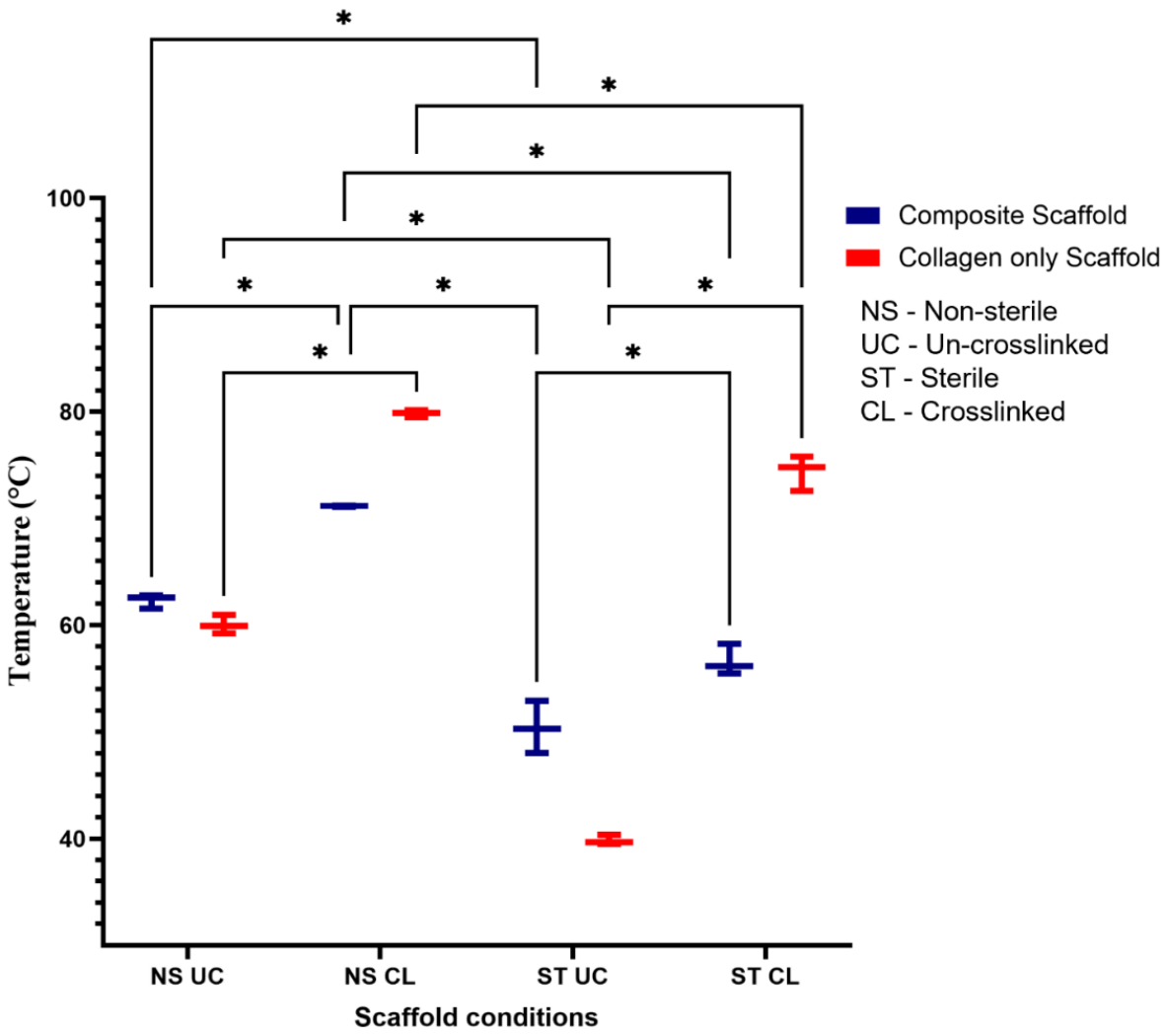

Figure 4.4: Denaturation temperature of collagen-only and composite scaffolds under four processing conditions. Box-and-whisker plots show the distribution of denaturation temperature (T_d) values for collagen-only and composite scaffolds across four processing conditions combining sterility and crosslinking, yielding a total of eight groups (n=3). Each box represents the interquartile range with the median indicated, and whiskers denote the full data range.

A significant row × column interaction was detected, accounting for approximately 18.88% of the total variation ($p = 0.0016$). This interaction indicates that the effect of processing condition on T_d depended on scaffold material type, and that the pattern of denaturing temperature changes across the four processing conditions was not identical for collagen-only versus composite scaffolds.

In summary, the box-and-whisker visualization and two-way ANOVA demonstrate that denaturing temperature varied systematically with both processing condition and scaffold material type, with a strong main effect of processing, a smaller but significant effect of material type, and a notable interaction between these factors.

4.3 Elastic behavior results

The tensile behavior of the scaffold groups was evaluated by uniaxial testing, and the resulting stress-strain responses are summarized in Figure 4.5. Because these specimens were tested in their dry state, their load-bearing capacity reflects the intrinsic stiffness of the collagen network, resulting in elastic moduli and ultimate tensile strengths within the megapascal range. Across all conditions, the scaffolds exhibited a characteristic collagenous tensile response, beginning with a non-linear toe region followed by a linear elastic region and eventual failure. The presence and extent of these regions varied among the eight scaffold conditions, indicating that scaffold composition, crosslinking, and sterilization influenced the mechanical response.

For the collagen-only scaffolds, the un-crosslinked non-irradiated group exhibited an elastic modulus of 706.9 ± 102.7 MPa and an ultimate tensile strength (UTS) of 32.8 ± 4.6 MPa, with a strain at fracture that varied between 6-15%. After EDC/NHS crosslinking, the elastic modulus changed to 422.8 ± 80.2 MPa, the UTS changed to 22.04 ± 3.03 MPa, and the strain at fracture ranged from 6 to 10%. In the irradiated collagen group, the un-crosslinked scaffolds exhibited an elastic modulus of 423.3 ± 4.31 MPa and a UTS of 15.36 ± 4.7 MPa. In comparison, the crosslinked scaffolds exhibited an elastic modulus of 824.5 ± 32.4 MPa and a UTS of 20 ± 5.4 MPa.

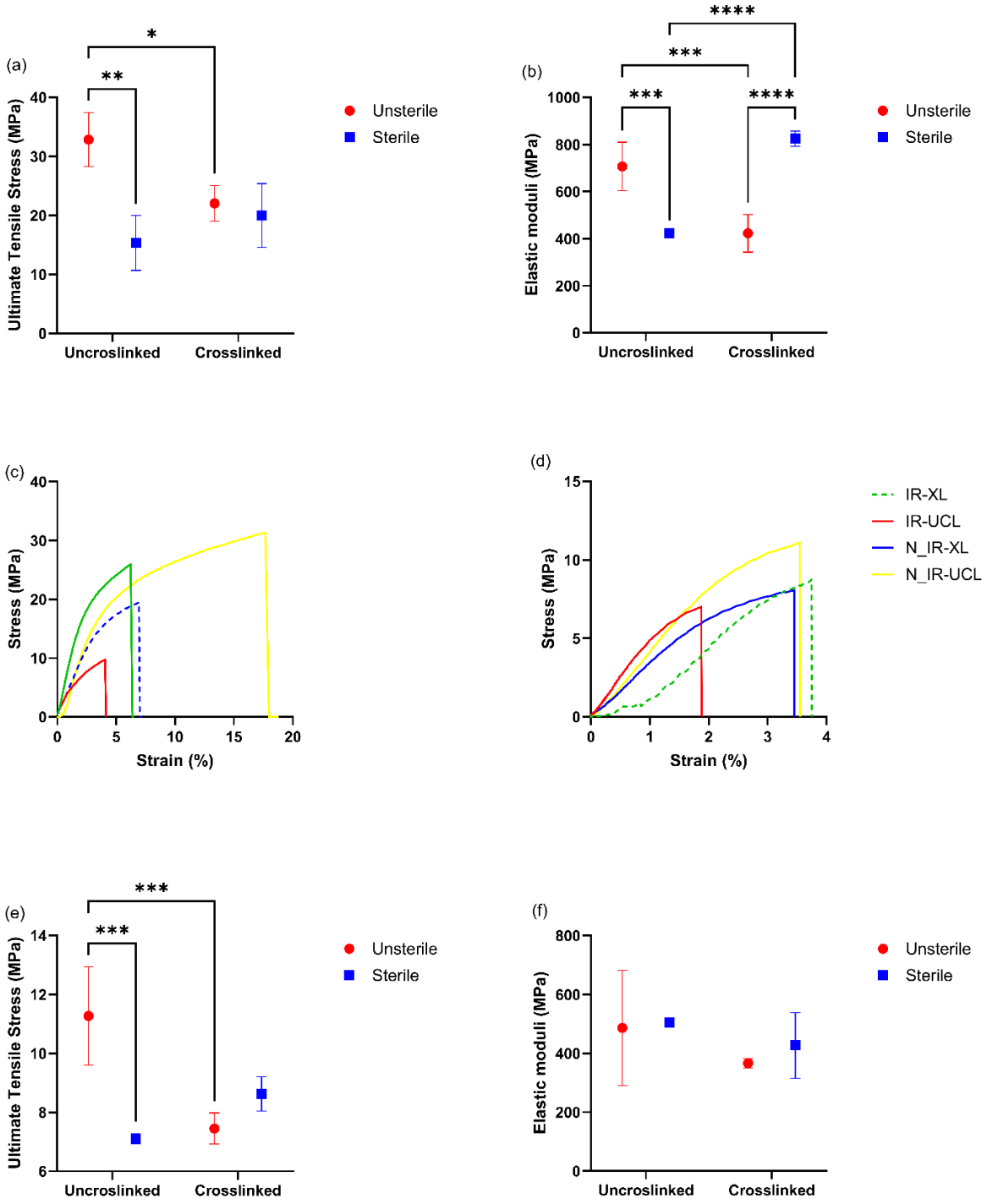

Figure 4.5: Mechanical properties of collagen and composite 2D films under different sterilization and crosslinking conditions. (a) Ultimate tensile strength (UTS) of collagen films as mean ± standard deviation. (b) Elastic moduli of collagen films presented as mean ± standard deviation. (c) Representative stress-strain curves of collagen films under four conditions: N_IR-UCL (non-irradiated, un-crosslinked, Blue), N_IR-XL (non-irradiated, crosslinked, Red dotted), N_IR-UCL (irradiated, un-crosslinked, Orange), and IR-XL (irradiated, crosslinked, Black dotted). (d) Representative stress-strain curves of composite films under the same four conditions. (e) Ultimate tensile strength (UTS) of composite films as mean ± standard deviation. (f) Elastic moduli of composite films presented as mean ± standard deviation. Statistical significance is indicated where applicable ($p < 0.005$); $n = 3$ for all groups.

For the composite scaffolds, the un-crosslinked non-irradiated group exhibited an elastic modulus of 486.5 ± 193 MPa and a UTS of 11.3 ± 1.66 MPa. Post-crosslinking, the composite scaffolds showed an elastic modulus of 366.4 ± 16.24 MPa, a UTS of 7.45 ± 0.53 MPa. In the irradiated composite group, the un-crosslinked scaffolds exhibited an elastic modulus of 505.3 ± 6.14 MPa and a UTS of 7.1 ± 0.17 MPa. In contrast, the crosslinked scaffolds exhibited an elastic modulus of 426.8 ± 112.4 MPa and a UTS of 8.63 ± 0.58 MPa. The strain at fracture for the composite scaffolds was generally lower than that of the collagen-only scaffolds, ranging from approximately 1-3% in the un-crosslinked state to approximately 3-4% in the crosslinked state.

Across the dataset, sterilization and crosslinking produced condition-dependent changes in mechanical performance. In some groups, crosslinking increased stiffness relative to the un-crosslinked state (irradiated collagen E: 423 (un-crosslinked) vs. 825 (crosslinked)), whereas in other groups the opposite trend was observed. The effect of sterilization also varied depending on whether the scaffolds were crosslinked, indicating an interaction between the two processing steps. This interaction was most evident in the collagen scaffolds ($p < 0.0001$), where sterilization altered the elastic modulus more strongly in the un-crosslinked state than in the crosslinked state. The composite elastic modulus showed no significant interaction, $p > 0.16$.

The stress-strain curves for the crosslinked groups consistently showed a non-linear toe region before the linear elastic region. In contrast, this region was less pronounced or absent in several of the un-crosslinked groups. The toe region was observed across all crosslinked scaffolds and reflected the initial uncrimping and alignment of collagen fibers under load. The transition into the linear elastic region occurred at approximately 1.75- 3% strain for the crosslinked collagen scaffolds and 0.4–2.5% strain for the crosslinked composite scaffolds, although this threshold varied slightly among conditions.

Among the crosslinked collagen scaffolds, the non-irradiated group exhibited an elastic modulus of 423 MPa, and the irradiated group exhibited an elastic modulus of 825 MPa. The corresponding UTS values were 22 MPa and 20 MPa, respectively. For the composite scaffolds, the non-irradiated crosslinked group exhibited an elastic modulus of 367 MPa, and the irradiated crosslinked group exhibited an elastic modulus of 427 MPa. In comparison, UTS values were 7.45 MPa and 8.63 MPa, respectively. These results show that both material type and processing history influenced the tensile response of the scaffolds.

Overall, the elastic behavior data demonstrate that scaffold stiffness, strength, and extensibility were strongly affected by the combined effects of crosslinking and sterilization. The collagen-only scaffolds generally showed greater extensibility than the composite scaffolds, while the composite scaffolds tended to fail at lower strains. The differences among the eight scaffold conditions suggest that the mechanical response depended not only on scaffold formulation, but also on the interaction between irradiation and crosslinking.

4.4 Enzymatic degradation of type 1 collagen

4.4.1 Preliminary 5-day Degradation results

Enzymatic degradation of type 1 collagen through collagenase synthesized from Clostridial histolyticum was initially performed over a preliminary 5-day period to evaluate how irradiation and EDC/NHS crosslinking influence the stability of collagen films and composite scaffolds. Scaffold mass loss was monitored at 24-hour intervals without replacing the enzyme solution between time points. Under these conditions, most of the measurable degradation occurred within

the first 24 hours, after which the mass loss curves plateaued for both collagen and composite scaffolds.

Collagen-only scaffolds showed clear separation between processing conditions: sterile un-crosslinked collagen degraded rapidly, reaching ~25% mass remaining at Day 3, whereas sterile and unsterile crosslinked collagen retained 95-99% of its mass throughout the entire period (Figure 4.6). Composite scaffolds, which contained 50% collagen and 50% elastin/hydroxyapatite, exhibited a more moderate degradation overall. Among irradiated composites, crosslinking produced minimal additional stabilization, with both sterile un-crosslinked and sterile crosslinked groups retaining ~35-53% of their mass. In contrast, non-sterile composites demonstrated a clear crosslinking effect: non-sterile un-crosslinked scaffolds degraded most rapidly (33-44% mass remaining), while non-sterile crosslinked scaffolds retained 45-69% of their mass.

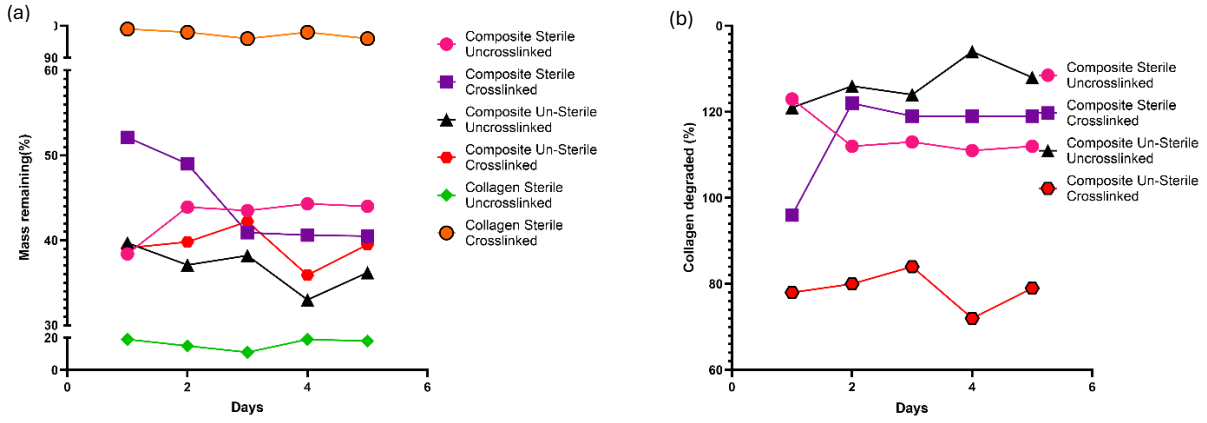

Figure 4.6: Enzymatic degradation of collagen-based scaffolds over five days. (a) Percentage of mass remaining for all sterile scaffolds and non-sterile composite scaffolds following incubation in collagenase for five days. (b) Percentage of collagen degraded in composite scaffolds across all four processing conditions (sterile crosslinked, sterile un-crosslinked, non-sterile crosslinked, non-sterile un-crosslinked). Values are normalized to the initial collagen content of each composite scaffold. Data represent n = 2, shown as mean ± SD.

These preliminary data show only qualitative trends in relative susceptibility to enzymatic degradation and did not support reliable estimation of degradation half-life, due to the apparent loss of enzyme activity over time and the resulting absence of continued mass loss beyond the initial 24-hour period. Collagen-specific normalization further highlighted this issue Figure 4.6b, with un-crosslinked composites exceeding 100% collagen degradation and crosslinked composites showing variable values- patterns influenced as much by processing variability as by true enzymatic activity. These constraints made it clear that a more controlled kinetic approach was required to quantify degradation behavior.

4.4.2 24-hour time-resolved degradation experiment

To obtain quantitative degradation kinetics, a second experiment was performed in which scaffold mass was recorded over 24 hours with measurements at 3, 6, 9, 12, and 24 hours. In this experiment, collagenase exposure was limited to 24 hours, and mass loss was tracked across the designated time points for all scaffold conditions. The resulting degradation profiles showed a progressive decrease in scaffold mass over the first 24 hours, with the largest changes occurring at earlier time points and approaching an apparent plateau by 24 hours.

The degradation curves were fitted using a one-phase exponential decay model, yielding estimates of degradation half-life and rate constant (k) for each collagen condition. The fitted curves captured the observed time-dependent mass loss and allowed quantitative comparison of degradation rates among the collagen scaffold groups.

For the collagen-only scaffolds, the normalized remaining mass decreased with time for all processing conditions. Non-linear regression of the 24-hour degradation kinetics revealed clear differences in the enzymatic susceptibility across material, irradiated state, and crosslinking conditions. Allowing the degradation rate constant K to vary between groups significantly improved the model fit ($F(3,20) = 31.75$, $p < 0.0001$), indicating that the four conditions—N_IR-UCL, N_IR-XL, IR-UCL, and IR-XL—degraded at measurably different rates. The superiority of the variable-K model confirms that at least one scaffold group exhibited a distinct degradation kinetic profile relative to the others. The appropriate equation for the degradation constant was used.

$$Y(t) = 100e^{-kt}$$

The un-crosslinked collagen scaffolds degraded rapidly, with the non-sterile losing half their mass within ~3.5 hours and the sterile with a half-life of ~2.9 hours. Their crosslinked counterpart, regardless of sterility, exhibited significantly slower degradation, with half-lives exceeding 11 days. Sterilization alone did not sustainably alter degradation in un-crosslinked collagen (K: 0.1988 vs 0.2370), but in crosslinked collagen, both NS-CL and ST-CL showed similar low-rate constants (~0.002), with an overlap in Figure 4.7a, indicating that crosslinking dominated the degradation response.

Initially, composite scaffolds were analyzed using the same model as collagen. Like collagen, the un-crosslinked composites, regardless of sterility, degraded rapidly, with half-lives of 3-4 hrs. Crosslinking reduced degradation substantially (half-lives of ~16-25 hours), though the magnitude of stability was significantly less than in collagen-only scaffolds, as shown in Figure 4.7a-b. However, since collagen only makes up 50% of the composition for the composite scaffolds, this

degradation behavior was analyzed as a bulk material, as the enzyme, Clostridial histolyticum collagenase, is specific to collagen and cannot degrade elastin and hydroxyapatite.

To reflect the 50% collagen content of the composite formulation, the degradation plateau in the exponential decay model was constrained to 50% of the initial mass. Under this constraint, the one-phase exponential decay fitting yielded adjusted estimates of degradation half-life and rate constant (K) for the composite scaffolds, corresponding to degradation of the collagen fraction within the composite.

Therefore, a secondary analysis was performed with constraints added to limit the degradation plateau to 50%, which accounted for the fact that only 50% of the composite mass is enzymatically degradable, yielding the biologically appropriate equation:

$$Y(t) = 50 + 50\, e^{-Kt}$$

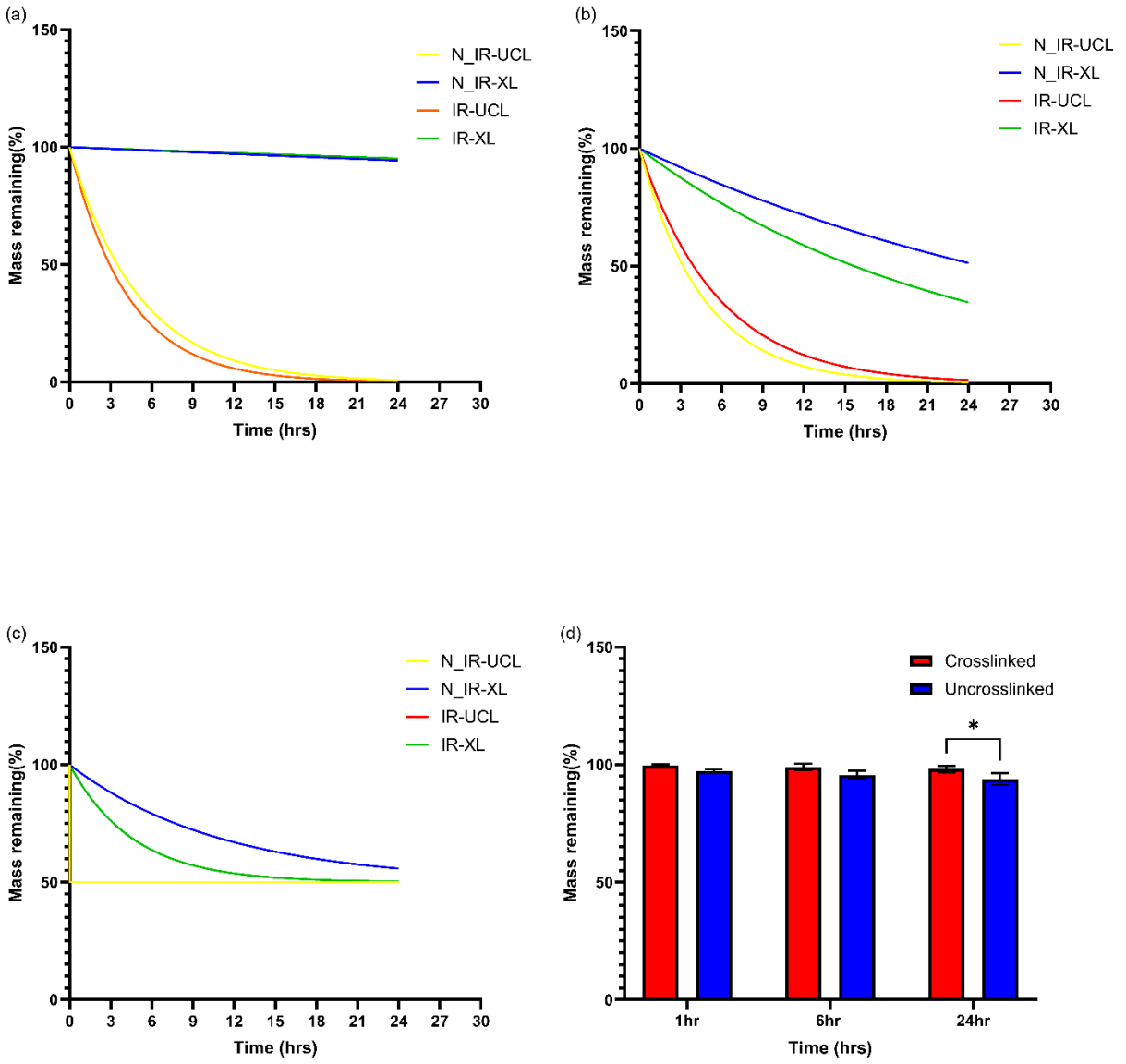

Figure 4.7: In vitro enzymatic degradation of collagen-based scaffolds over 24 hours. (a) Percentage of mass remaining for collagen-only scaffolds under four processing conditions: N_IR-UCL (non-irradiated, un-crosslinked; yellow), N_IR-XL (non-irradiated, crosslinked; blue), IR-UCL (irradiated, un-crosslinked; orange), and IR-XL (irradiated, crosslinked; green). (b) Percentage of bulk mass remaining for composite scaffolds under the same four conditions. For panels (a) and (b), solid lines represent a non-linear regression fit using a first-order, one-phase exponential decay model constrained to a baseline of 100% and a plateau of 0%. (c) Percentage of collagen-normalized mass remaining for composite scaffolds under the same four processing conditions. Experimental data represent mean ± SD (n = 3). Solid lines represent a non-linear regression fit using a first-order, one-phase exponential decay model constrained to a baseline of 100% and a plateau of 50%. (d) Composite control samples incubated in Tris buffer containing 5 mM $CaCl_2$, washed after 1 hour and 24 hours, shown for crosslinked (red) and un-crosslinked (blue) scaffolds (n = 3).

Under this corrected model, crosslinking significantly reduced the degradation rate of the collagen fraction (NS-CL: K = 0.08995, ST-CL: K = 0.2161). At the same time, the un-crosslinked composites, irrespective of irradiated state, degraded too rapidly for stable kinetic parameter estimation (Figure 4.8). A comparison of fits showed that allowing separate rate constants K for N_IR-UCL, N_IR-XL, IR-UCL, and IR-XL provided a better description of the data than a shared-k model ($F(3,36) = 4.496$, $p = 0.0088$). The non-sterile crosslinked composite scaffolds (NS-CL) exhibited a half-life of 7.71 h, while the sterile crosslinked composite scaffolds (ST-CL) exhibited a half-life of 3.21 h. The fits for the un-crosslinked composite conditions were less stable, reflecting the rapid mass loss.

Across the four experimental analyses (DSC, FTIR, elastic behavior, and enzymatic degradation), X-ray sterilization and EDC/NHS crosslinking produced condition-dependent changes in denaturation temperature, molecular structure, mechanical response, and collagenase degradation kinetics. These findings form the basis for the discussion section, which will examine how processing history governs scaffold thermomechanical and degradation behavior in this set of experiments. Additional results and a separate Discussion for two further collagen batches, undertaken to evaluate batch-to-batch variability, will be appended to the thesis and are not considered in the main analysis here.

Chapter 5: Discussion

5.1 Molecular analysis

FTIR spectroscopy was used to assess how X-ray sterilization and EDC/NHS crosslinking affected the molecular structure of the collagen-only and composite scaffolds. The presence and condition-dependent changes of the characteristic amide bands (Amide I, II, and III) provided information about triple-helix integrity, crosslinking state, and processing-induced modifications of the collagen network.

5.1.1 Collagen scaffolds

In the collagen-only scaffolds, the Amide I band (C=O stretching vibrations, 1630–1660 cm^{-1}) showed clear condition-dependent shifts (Figure 4.1). While all values fall within the range associated with intact triple-helix collagen, the downward shift after sterilization indicates that X-ray treatment altered the collagen environment, and the larger shift in the sterilized crosslinked group suggests a stronger structural effect in that condition.

The Amide II band (1540–1560 cm^{-1}) showed a downward shift from the non-irradiated scaffolds to the irradiated groups, consistent with changes in hydrogen-bonding and local secondary structure. The Amide III band (~1235–1245 cm^{-1}) remained well defined in the un-crosslinked scaffolds but decreased in intensity and broadened following crosslinking, regardless of irradiation. This reduction in Amide III intensity reflects crosslinking-induced alterations in collagen secondary structure, likely arising from restricted chain mobility and changes in N–H bending and C–N stretching associated with newly formed covalent bonds. The combined broadening and intensity loss in Amide III support the interpretation that sterilization disrupts the

triple helix, with crosslinking limiting the altered network rather than fully restoring the native structure.

A distinct absorption band centered near ~1770 cm^{-1} appeared exclusively in the sterilized groups and was absent in the non-irradiated scaffolds (Figure 4.1). This feature is consistent with radiation-induced carbonyl formation, arising from free-radical oxidation pathways in which reactive oxygen species generate hydroperoxides that decompose into carbonyl-containing products. The presence of this band aligns with reports of oxidative carbonyl damage following ionizing-radiation exposure and confirms that X-ray sterilization introduces chemical modifications beyond purely thermal denaturation.

Overall, consistent with its role as a zero-length crosslinker, EDC/NHS produced only modest changes in the Amide I, II, and III profiles in non-sterile collagen scaffolds. Because the crosslinker forms covalent bonds between existing functional groups, the overall collagen spectra in the non-irradiated crosslinked state remained largely similar to their un-crosslinked counterparts, with more subtle shifts and broadening rather than the emergence of new bands.

5.1.2 Composite scaffolds

In the composite scaffolds, the Amide I band (C=O stretching, 1630–1660 cm^{-1}) was observed at 1641 cm^{-1} for the non-irradiated crosslinked and un-crosslinked composite scaffolds, at 1639 cm^{-1} for the irradiated un-crosslinked scaffolds, and at 1631 cm^{-1} for the irradiated crosslinked composites. All values lie within the collagen Amide I range and are therefore compatible with a preserved triple-helix structure. However, the downward shift in the sterile crosslinked group toward ~1630 cm^{-1} suggests partial thermal denaturation induced by X-ray sterilization, with subsequent stabilization of the altered network through crosslinking. Once thermal denaturation

has occurred, subsequent crosslinking appears unable to fully reverse or mitigate the antagonistic effects on secondary structure, instead stabilizing a structurally modified collagen network.

The Amide II band (N–H bending/C–N stretching, 1540–1560 cm^{-1}) showed the most pronounced changes in the composite group. In the non-irradiated composites, both the crosslinked scaffold (1548 cm^{-1}) and the un-crosslinked scaffold (1546 cm^{-1}) fall within the accepted collagen range. In the irradiated composites, only the un-crosslinked scaffold (1541 cm^{-1}) remains within this range, whereas the irradiated crosslinked composite shifts ~10 cm^{-1} below the typical collagen interval to ~1529 cm^{-1}. This downward shift can reflect the combined effect of new amide formation due to EDC/NHS crosslinking and potential overlap with elastin absorptions near 1520–1530 cm^{-1}, as elastin exhibits its Amide II band around 1520 cm^{-1}. Such overlap would be consistent with the presence of elastin or elastin-like components within the composite matrix.

Across the composite scaffolds, X-ray sterilization produced modest shifts in Amide I and more pronounced shifts in Amide II, particularly in the crosslinked groups. In the un-crosslinked composites (NS-UC and ST-UC), sterilization shifted the Amide I band by ~2 cm^{-1} and the Amide II band from ~1548–1546 cm^{-1} to ~1541 cm^{-1}, indicating thermal denaturation of collagen in the absence of crosslinking. Crosslinking of the sterilized composite scaffolds produced the largest wavelength changes (Amide I: ~10 cm^{-1}; Amide II: ~17 cm^{-1}), suggesting that crosslinking after sterilization confers partial structural compensation for irradiation-induced damage but also further modifies the local bonding environment. This interpretation is supported by DSC analysis, which showed corresponding changes in denaturing temperature for these conditions.

In the mineral phase, the ν_4 PO_4^{3-} bending doublet and O–H liberation band were present across all composite conditions, confirming preserved hydroxyapatite crystallinity and intact hydroxyl

channels. The upward shift of the ν_1 PO_4^{3-} symmetric stretch—from ~960 cm^{-1} in the NS-UC scaffold to ~977 cm^{-1} in the other composite conditions—suggests increased hydroxyapatite crystallinity, potentially driven by crosslinking and/or X-ray sterilization, with possible minor contributions from overlapping organic bands. These changes in the inorganic signature indicate that processing steps influence not only the collagen matrix but also the mineral environment, which may contribute to the distinct thermal and mechanical behavior observed in the composite scaffolds. Overall, FTIR analysis indicates that X-ray sterilization and EDC/NHS crosslinking alter the molecular structure of collagen within the scaffolds, and these structural modifications support the thermomechanical and degradation behaviors discussed in the subsequent sections.

5.2 Thermal property analysis

In this study, the denaturation temperature (T_d) provided a measure of thermal stability of the collagen network within the scaffolds. An increase in Td is generally associated with improved molecular stability and higher crosslink density. In contrast, a reduction suggests a disruption in the triple helical structure of collagen or compromised structural integrity. Across the eight scaffolds and processing conditions, the observed T_d shifts reflect the combined influence of X-ray sterilization and EDC/NHS crosslinking on collagen stability.

5.2.1 Effect of Irradiation on the scaffold

Irradiation influences the thermal transition of both the collagen and composite scaffolds. Within the same composition and crosslinking state, irradiated samples exhibited denaturation temperatures that differed from the non-irradiated ones. However, in all groups, irradiation led to a slight to moderate reduction in T_d when compared with their non-irradiated counterparts within the same group. This effect was more pronounced in collagen-only scaffolds, where the sterile, un-

crosslinked samples exhibited a much lower Td than the non-irradiated, un-crosslinked samples. Additionally, within collagen, the irradiated un-crosslinked and irradiated crosslinked groups showed a very large disparity in denaturation temperature (approximately 39.85 ± 0.44 °C and 74.39 ± 1.68 °C), indicating that the combination of irradiation with crosslinking produced a substantial recovery and enhancement of thermal stability compared to irradiation alone.

In contrast, the difference in denaturation temperature between non-irradiated crosslinked and sterile crosslinked collagen scaffolds was small, at less than 5 °C, suggesting that the impact of irradiation was minimal once crosslinking was introduced. A similar pattern was observed in the composite scaffolds, where irradiated crosslinked and non-irradiated crosslinked scaffolds differed by only about 10°C in denaturation temperature. This confirms that crosslinking offsets the destabilizing effect of X-ray irradiation.

5.2.2 Effect of crosslinking within each composition and sterility state

Within each scaffold type and sterility condition, crosslinked scaffolds consistently exhibited higher denaturing temperatures compared to their un-crosslinked counterparts. For both scaffold material types, the transition from un-crosslinked to crosslinked produces an upward shift in Td, visible as the higher bar in Figure 4.4 for the crosslinked groups. This behavior is consistent with the expected formation of additional covalent bonds between collagen chains, which reduces molecular mobility and stabilizes the triple helix structure of the collagen fibers[86].

However, the magnitude of increase in the T_d for the crosslinked specimens is not identical across all conditions. In some cases, crosslinking produces a large increase in $T_{d,}$ while in others, the increase is less pronounced, as shown in Figure 4.4 for the irradiated composite. This variability suggests that the extent of crosslink formation might be influenced by the scaffold's composition

and prior irradiation, which might have induced chain scission in the scaffold polymer, slightly altering the collagen network and leading to different thermal outcomes compared with non-irradiated scaffolds[102]. As irradiation and crosslinking do not act uniformly across all compositions and crosslinking, it reinforces the conclusion that the effects of processing steps are interdependent.

5.2.3 Combined Effect of irradiation and crosslinking

Across all eight conditions, the combined effects of the collagen-based scaffold composition, sterility, and crosslinking produced tunable denaturation temperatures and enthalpy values. The aim is to achieve an appropriate denaturation temperature rather than simply maximal denaturation. While non-irradiated scaffolds generally displayed the highest T_d values, these conditions are not suitable for implantation and only partially reflect laboratory in vitro practice because ethanol-based handling does not guarantee the required sterility for clinical use. In contrast, the X-ray sterilized scaffolds represent a terminal sterilization technique, hence providing a more relevant benchmark for in vivo applications.

With this clinically relevant benchmark, crosslinking acts as a stabilizing force compensating for the destabilization induced by irradiation to allow the denaturation temperature to remain sufficiently above physiological temperatures. The ‘optimal scaffold’, the crosslinked sterile composite scaffold, has a denaturation temperature of 56.62 ± 1.42 °C, providing an approximately 20 °C safety margin above the normal physiological temperature of 37 °C. This indicates that the collagen network will remain thermally stable during cell culture and under normal and abnormal in vivo conditions. This level of thermal stability is important for preserving scaffold architecture and mechanical integrity during cell seeding, proliferation, and differentiation.

The fact that the highest T_d values are found in the non-irradiated scaffolds, which are not clinically acceptable for implantation, underscores that the goal of optimization is not to maximize the denaturation values but rather to tune them within an acceptable range that is compatible with both biological function and mechanical requirements of the target tissue

5.3 Elastic behavior

In tensile testing, the scaffolds exhibited characteristic collagenous stress–strain behavior, with an initial non-linear toe region followed by a linear elastic region and eventual failure. The elastic modulus, ultimate tensile strength (UTS), and strain at fracture varied systematically across the eight scaffold conditions, indicating that scaffold composition, crosslinking, and X-ray sterilization strongly influenced mechanical performance.

EDC/NHS crosslinking influenced mechanical behavior in a condition-dependent manner. In the unsterile collagen and composite scaffolds, crosslinking reduced elastic modulus and UTS, suggesting increased network constraint and reduced deformability. In sterile collagen scaffolds, crosslinking instead increased modulus, implying that irradiation altered the collagen network in a way that made the crosslinked structure stiffer. For the composite scaffolds, crosslinking had a smaller effect on modulus but tended to reduce tensile strength, which can be attributed to a brittle hydroxyapatite-containing network, where hydroxyapatite acts as a stress concentrator.

Sterilization showed a strong interaction with crosslinking in collagen scaffolds, reducing modulus in un-crosslinked samples but increasing modulus in crosslinked samples. This indicates that X-ray sterilization weakens collagen when no chemical stabilization is present, but its effects are partially compensated by EDC/NHS crosslinking. In the composites, sterilization produced only modest changes, suggesting that the composite architecture is less sensitive to irradiation. Overall,

the results show that crosslinking and sterilization do not act independently, but together shape the stiffness, strength, and failure behavior of the scaffolds.

In summary, crosslinking and sterilization jointly did not produce any singular trend; the dominant pattern is interaction-driven. The mechanical effect depends on the crosslinking state and the effect of crosslinking on the sterilization state. In the collagen specimens, this is most pronounced in the interaction exhibited in the elastic moduli: sterilization decreased stiffness in the un-crosslinked scaffold but increased it in the crosslinked scaffold. For the composite scaffold, the interaction is absent in the elastic moduli. Yet, the UTS exhibits an interaction where UTS is lower in un-crosslinked samples and higher in crosslinked samples, as reported in the literature.

5.4 Enzymatic degradation

Enzymatic degradation showed that scaffold breakdown was strongly dependent on crosslinking status and, in the composite groups, on how the plateau was modeled. In the collagen-only scaffolds, un-crosslinked samples degraded rapidly in collagenase, with short half-lives. In contrast, crosslinked samples were much more resistant, indicating that EDC/NHS crosslinking substantially reduced enzymatic accessibility of the collagen network. This is consistent with literature that shows crosslinking increases resistance to collagenase by limiting fibril mobility and reducing the number of accessible cleavage sites[103].

For the composite scaffolds, degradation was also faster in the un-crosslinked state and slower after crosslinking. The plateau was constrained to represent the collagen fraction of the composite, as collagenase primarily targets collagen, so the non-collagen phase should remain largely intact and contribute to the residual mass. Overall, the degradation data complement the FTIR, DSC, and tensile results by showing that the same processing steps that alter collagen structure and

thermomechanical behavior also control susceptibility to enzymatic breakdown. In other words, crosslinking improved enzymatic stability, while sterilization and composite formulation modulated how strongly that protection was expressed.

5.5 Streamlined physicochemical and thermomechanical assessment

Overall aim of this project was not only to determine how X-ray sterilization and EDC/NHS crosslinking altered the thermomechanical and degradation behavior of the scaffolds, but also to evaluate whether one measurement could serve as a practical predictor of the others. In this framework, DSC was treated as the primary reference because denaturing temperature reflects the stability of the collagen network and provides a quantitative indicator of molecular integrity. The FTIR, tensile, and enzymatic degradation results were then interpreted relative to the DSC findings to determine whether structural changes detected spectroscopically were translated into measurable differences in stiffness, failure behavior, and collagenase susceptibility. This approach is particularly relevant for collagen-based biomaterials, where the same processing step can influence molecular structure, thermal stability, mechanical performance, and biodegradation in a coupled manner.

Across the dataset, the results show that DSC can serve as a useful anchor for estimating broader scaffold behavior, but only when source variability is considered. Conditions that exhibited higher Td generally also showed FTIR features consistent with a more stabilized collagen network, increased stiffness under tensile loading, and greater resistance to enzymatic degradation. In contrast, lower Td conditions were associated with spectral signs of collagen disruption, reduced mechanical stability, and faster collagenase-mediated mass loss. At the same time, the magnitude and even direction of some processing effects depended on the collagen batch, highlighting that

batch-to-batch variability can meaningfully alter the thermomechanical response. This is consistent with prior reports showing that collagen source, age, and preparation history can influence fibril organization and mechanical properties. Therefore, the broader objective is not simply to predict one property from another, but to build a model that uses DSC as a standardized reference to estimate a range of thermomechanical outcomes across collagen batches, while accounting for the inherent variability of the starting material.

5.6 Limitations of the study

Several methodological limitations should be considered when interpreting the present results. For the FTIR analysis, the absence of purge gas may have introduced additional atmospheric interference, and the use of ATR meant that variations in sample-crystal contact could have affected the measured absorbance and peak intensity. For DSC, the samples were analyzed in the wet state, but the water content of individual samples could not be measured directly; as a result, differences in hydration levels may have contributed to variability in the thermal response. In addition, environmental conditions were not identical across all experiments, which may have introduced minor variation between runs[104].

Sample-specific factors also influenced the mechanical testing data. Because the composite scaffolds were thin and heterogeneous, thickness varied along the film length, so an average of multiple thickness measurements was used to calculate stress. In addition, manual cutting introduced some edge irregularity, and the crosslinked scaffolds developed crimping after drying, which may have affected load distribution during tensile testing. For the enzymatic degradation assay, some mass loss may have occurred during washing and handling steps, particularly for the un-crosslinked scaffolds, which could affect the estimated rates of degradation. Despite these

limitations, the results still reveal clear trends in how sterilization and crosslinking affect scaffold thermomechanical behavior and degradation[88].

Chapter 6: Batch-to Batch Variability

This chapter presents a comparison of two independently fabricated batches from different lots of collagen-only and collagen–hydroxyapatite/elastin composite scaffolds. The study evaluated the effects of EDC/NHS crosslinking, irradiation, and batch variation on three endpoints (experiments): enzymatic degradation, uniaxial tensile properties, and differential scanning calorimetry (DSC)-derived thermal stability. Across both batches and scaffold types, the experimental design comprised of four treatment conditions non-irradiated un-crosslinked (N_IR-UCL), non-irradiated crosslinked (N_IR-XL), irradiated un-crosslinked (IR-UCL), and irradiated crosslinked (IR-XL).

The data, in line with literature, shows that the effects of scaffold processing, irradiation and crosslinking, are endpoint driven. Crosslinking controls enzymatic stability and thermal denaturation behaviour, whereas mechanical properties, in particular elastic modulus, was substantially more sensitive to batch-to-batch variation. Thus, the two batches reproduced the general direction of treatment effects, especially for composite scaffolds, but not to the same magnitude especially in the mechanical properties.

Several constraints must be identified when interpreting these findings. Degradation testing used destructive sampling, meaning each time point represented different specimens rather than repeated measures of the same scaffold. In addition, batch 2 used a significantly higher starting scaffold mass at the 24 h degradation time point, which altered the enzyme: substrate ratio and made this time point not directly comparable with the 3–12 h samples. Hence, the primary degradation analysis was restricted to the 3–12 h interval.

6.1 Degradation behaviour

Crosslinking was the dominant determinant of mass retention during collagenase degradation. In the ANOVA analysis of total mass remaining between 3 and 12 h, crosslinking accounted for 90.10% of the total variation in mass remaining ($F = 3230.18$, $p < 0.0001$). By comparison, batch accounted for 4.75% of total variation, while time accounted for 1.44%. The dominant influence of crosslinking indicates that EDC/NHS treatment was the principal factor controlling resistance to enzymatic mass loss.

Although the batch effect was statistically significant ($F = 170.42$, $p < 0.0001$), its magnitude was small relative to the crosslinking effect. Hence, the batch variation influenced the absolute scale of degradation, but it did not change the conclusion that crosslinking controls scaffold stability. Batch 2 retained more mass than batch 1, with an average bias of +8.83 percentage points across the 3–12 h comparison window.

Irradiation did not exert a significant overall main effect on degradation ($p = 0.740$); however, it participated in significant interactions with batch and crosslinking. Specifically, batch × irradiation, irradiation × crosslinking, and batch × irradiation × crosslinking interactions were statistically significant. This means that irradiation was not uniformly beneficial or harmful: its effect depended on whether scaffolds were crosslinked and on which manufacturing batch was evaluated. Because of the small sample size and observed heterogeneity of variance, these interaction effects should be interpreted as empirical rather than conclusive.

The sensitivity analysis including the 24 h time point further supports use of the restricted primary analysis window. When the batch-2 24 h data were included, the apparent contribution of batch increased from 4.75% to 7.50% of total variation, while the contribution of crosslinking declined

from 90.10% to 82.26%. This increase in apparent batch effect is consistent with the documented change in starting scaffold mass and enzyme: substrate ratio at 24 h.

6.2 Degradation mechanism

The degradation data also reveal that total mass loss cannot be interpreted simply as collagen degradation. The composite consisted of 50% collagen and 50% HA/elastin by mass, but all un-crosslinked composites lost more than 50% of their total mass. This finding demonstrates that mass loss exceeded the collagen fraction alone as the enzyme collagenase specifically targets collagen. This is attributed to the physical release of the HA/elastin phase after breakdown of the collagen network which could be physically seen.

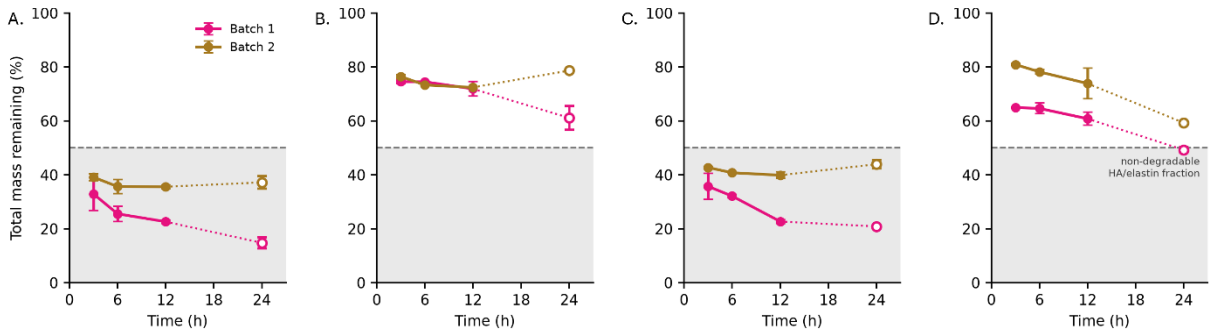

Figure 6.1: Composite scaffold degradation during collagenase exposure. Total mass remaining of composite scaffolds from batches 1 and 2: Composite scaffold degradation during collagenase exposure. Total mass remaining of composite scaffolds from batches 1 and 2: (A) non-irradiated, un-crosslinked (N_IR-UCL); (B) non-irradiated, crosslinked (N_IR-XL); (C) irradiated, un-crosslinked (IR-UCL); and **(D)** irradiated, crosslinked (IR-XL). Open symbols and dotted line segments indicate the 24 h observations. These measurements were excluded from the primary 3–12 h analysis because batch-2 specimens had a higher starting mass, resulting in a reduced enzyme: substrate ratio. The shaded region indicates the nominal 50% HA/elastin fraction of the composite scaffold.

By 3 hours, all un-crosslinked composite conditions had already reached complete loss of the collagen phase, Figure 6.1. At 12 hours, the retained HA/elastin fraction ranged from approximately 45% to 80%, depending on batch and irradiation condition. In batch 1, un-crosslinked composites lost approximately 20–35 percentage points of additional scaffold mass through mineral shedding; in batch 2, the corresponding loss was approximately 10–14 percentage points. The batch difference in un-crosslinked degradation was interpreted as a difference in network integrity and mineral retention rather than a difference in collagenase susceptibility.

This distinction has important implications. The degradation kinetics of un-crosslinked scaffolds were uncalculatable because complete collagen loss had already occurred by the earliest measured time point, 3 hours. Hence, the kinetic rate constant and half-life could not be estimated. Therefore, degradation kinetics were identifiable only for crosslinked composites. The current 3 hours first sampling point was inadequate for resolving the rapid degradation of un-crosslinked samples; future studies should include more time points prior to 3 hours, such as 15, 30, 60, and 120 min.

For crosslinked composites, the enzyme-resistant collagen fraction was more reproducible between batches than the fitted degradation rate constant. In the non-irradiated crosslinked condition, the estimated resistant collagen plateau was 46.1% in batch 1 and 45.1% in batch 2, a difference of only one percentage point. This indicates that crosslinking reproducibly established a resistant collagen fraction.

6.3 Mechanical and thermal properties

The mechanical and thermal analyses demonstrated that not all physicochemical measurements are reproducible. Thermal denaturation temperature (T_d) was the most reproducible endpoint, whereas elastic modulus and ultimate tensile strength (UTS) were more affected by batch-dependent variation. This is consistent with the distinction between chemistry-controlled and architecture-controlled scaffold properties.

Table 1: Percent of total sum of squares, three-way (batch × IR × XL) per endpoint. "Batch-related" pools the batch main effect and all three batch interactions (batch × IR, batch × XL, batch × IR × XL); the residual is the remainder to 100 %.

Material	Endpoint	XL (%)	IR (%)	IR × XL (%)	Batch-only (%)	Batch × XL (%)	Batch-related total (%)	Residual (%)
Collagen	E	25	0.5	2.8	16.2	32	53.1	18.6
Collagen	T_d	76.4	13.8	4	2.4	1.5	5.1	0.6
Collagen	UTS	31.5	3.1	3.1	0.5	17.1	30.3	32
Composite	E	42.9	0.2	0.3	14.9	11.9	27.5	29.1
Composite	T_d	25.6	69.7	0.03	0.1	1.6	3.9	0.8
Composite	UTS	5.8	7.3	20.6	29.7	0.02	31.9	34.4

For collagen-only scaffolds, batch-related terms accounted for 53.1% of the variance in elastic modulus. The batch × crosslinking interaction alone accounted for 32.0% of total variation, indicating that the stiffening effect of crosslinking differed substantially between the two batches. This is a critical because it means that a crosslinking-induced increase in modulus cannot be assumed to transfer quantitatively between batches. The most plausible explanation is variation in

architectural characteristics which can influence load transfer and deformation but are not fully captured by the chemical treatment alone.

The composite elastic modulus showed somewhat lower but still important batch dependence. Batch-related effects accounted for 27.5% of the variance in composite modulus, while the residual variation accounted for 29.1%. Compared to the collagen scaffolds, the composite scaffold displayed a batch-to-batch offset rather than a strong condition-dependent response. This suggests that mineral incorporation may reduce some variability in the crosslinking response. The UTS had an intermediate position. Batch-related effects accounted for approximately 30–32% of the total variance in UTS for both collagen-only and composite scaffolds.

Thermal denaturation temperature was substantially more significant. For collagen scaffolds, batch-related terms accounted for only 5.1% of the total variation in T_d, while treatment variables explained approximately 90% of the variance. For composite scaffolds, batch-related effects accounted for only 3.9%, and irradiation was the largest factor, explaining 69.7% of the total variation in T_d. As batch effects contributed the lowest percentage of total variance among the factors examined, the DSC results suggest that thermal stability was the most robust and transferable metric across all three endpoints, demonstrating greater consistency between batches than the corresponding mechanical or structural measurements.

6.4 Relationships among endpoints

This data does not support the use of thermal stability as a universal substitution for mechanical strength or enzymatic stability. Among all evaluated endpoints, the only statistically significant cross-endpoint relationship was between elastic modulus and UTS. This is expected because both

are uniaxial tensile measures taken together and portray related aspects of scaffold load-bearing behaviour. Reporting both measurements remains useful for distinguishing stiffness from failure strength, but they provide inadequate information within this small dataset.

In contrast, no significant statistical relationship was observed between thermal denaturation temperature and 12 hours mass remaining for composite scaffolds ($p = 0.210$). DSC primarily reports collagen molecular stability and crosslink-associated thermal resistance, whereas enzymatic degradation of the composite depends strongly on network connectivity and retention of the HA/elastin phase. An un-crosslinked composite may have a moderate T_d but still undergo rapid structural disintegration and mineral shedding when the collagen network is degraded. Therefore, denaturing temperature cannot be treated as a validated stand-alone substitution for enzymatic stability in the present dataset. This supports the interpretation that the physicochemical and mechanical endpoints measure related but non-interchangeable aspects of scaffold quality.

6.5 Batch transferability and Performance Index

To integrate scaffold performance with reproducibility, each formulation was positioned according to its Scaffold Performance Index (SPI) and Batch Reproducibility Index (BRI) (Figure 6.2). This analysis demonstrates that high performance and inter-batch reproducibility are related but distinct criteria; a formulation that performs well in one batch is not necessarily the most transferable formulation across batches.

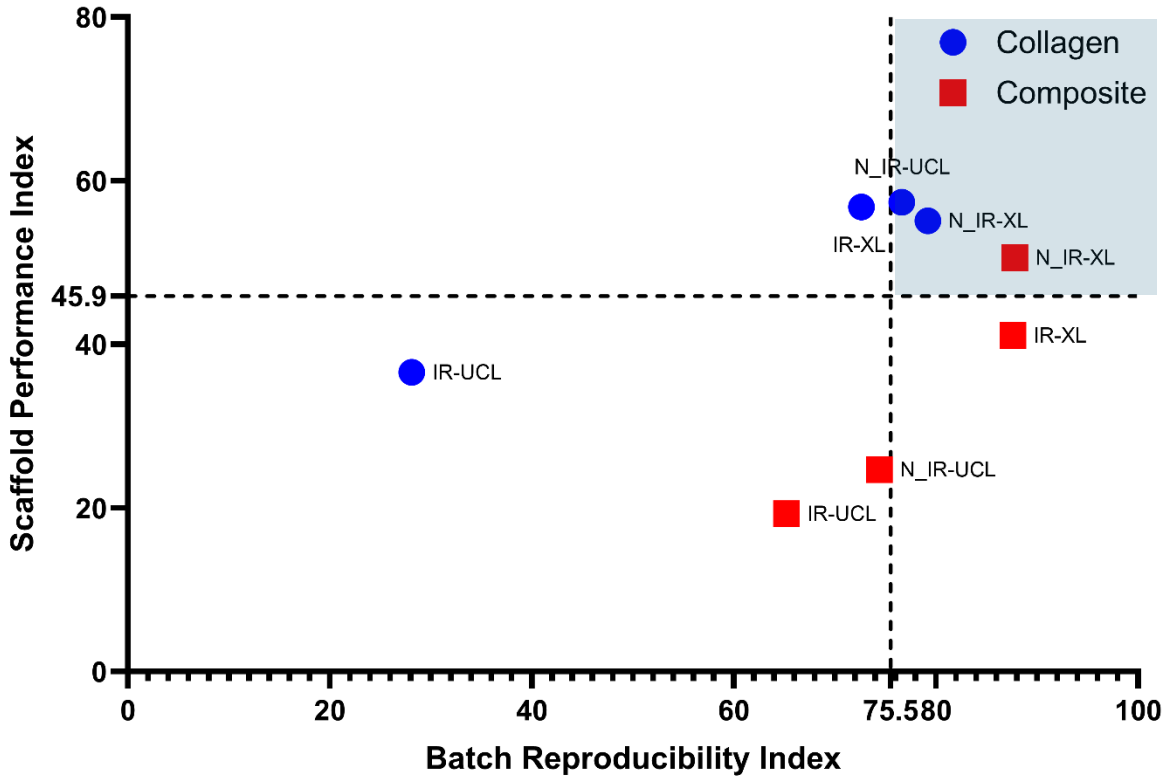

Figure 6.2: Integrated decision map of scaffold performance and batch reproducibility. Scaffold Performance Index (SPI) is plotted against the Batch Reproducibility Index (BRI) for collagen-only and collagen–HA/elastin composite scaffolds. Higher SPI values indicate stronger overall performance across the available endpoints, whereas higher BRI values indicate closer agreement between batches. Dashed lines indicate median thresholds used to define the performance and reproducibility quadrants. The blue shaded upper-right quadrant identifies conditions that combine above-median scaffold performance with above-median batch reproducibility.

The integrated performance analysis indicated that composite scaffold conditions were more transferable between batches than collagen-only conditions. Both batches identified crosslinked composites as superior to un-crosslinked composites, and both ranked the non-irradiated crosslinked composite as the highest-performing composite condition, Figure 6.2.

Nevertheless, only the irradiated crosslinked composite (IR-XL) met all pre-specified batch-transferability criteria: mean absolute inter-batch relative difference of 15% and preservation of within-material rank order. Its mean relative difference was 10.1%, and its composite rank was

maintained in both batches. The non-irradiated crosslinked composite (N_IR-XL) produced the strongest overall composite performance score and showed exceptionally low inter-batch variation in degradation for the non-irradiated crosslinked state, with an inter-batch coefficient of variation of 1.15%. However, it did not meet the full transferability criteria because of larger differences in some mechanical endpoints.

Un-crosslinked composites should not be advanced based on the present results. They showed rapid collagen loss, physical mineral shedding, poor integrated performance, and incomplete kinetic interpretability under the present sampling schedule. Their degradation profile does not represent a controllable degradation mechanism but rather collapse of the collagen network and subsequent release of the non-collagen phase.

The major limitation in making a standardisation claim is the number of batches and specimens. With only two batches, the estimated between-batch standard deviation has a relative standard error of ~71%. This means that batch variation can be observed but within this limited dataset, cannot be quantified.

Chapter 7: Conclusion and Future Work

In summary, this thesis investigated the physiochemical, thermomechanical, and degradation properties of collagen-based scaffolds to support optimal scaffold design. The overarching aim was to determine whether a single experiment could be used to infer other scaffold properties across collagen batches when processing conditions were held constant. Based on this limited dataset, a fully standardized method to estimate mechanical properties from limited physicochemical testing cannot yet be established. The evidence supports a more limited conclusion: thermal denaturation temperature is relatively reproducible between batches and is sensitive to crosslinking and irradiation chemistry, but it does not reliably predict elastic modulus, ultimate tensile strength, or enzymatic stability. Mechanical properties were strongly influenced by batch-dependent structural features that are not adequately represented by the available physicochemical measurements (DSC).

Therefore, the present data can support development of a screening framework but cannot justify replacing direct mechanical testing with a standardized predictive method based on limited physicochemical testing alone. Establishing such a method would require a larger multi-batch dataset, direct quantification of scaffold architecture, matched physicochemical and mechanical measurements, adequate replication, and external validation of predictive models across independently manufactured scaffold batches.

The present study provides preliminary evidence that crosslinking, irradiation, and fabrication batch can influence scaffold degradation, thermal stability, and mechanical behaviour in distinct ways. However, the limited number of batches and specimens prevents the establishment of a validated substitution method for estimating mechanical properties from physicochemical measurements alone. Future work should therefore expand the degradation time course, increase manufacturing replication, quantify batch-level variability, and validate scaffold performance in

the three-dimensional model using biologically relevant targets associated with the trabecular bone–bone marrow environment. The expanded study should quantify the independent and interacting effects of EDC/NHS crosslinking, irradiation sterilization, and fabrication variability on degradation resistance, elastic modulus, and UTS. These results can then be used to define ranges and optimize scaffold processing parameters for the intended application. Additional studies should evaluate cell viability and stem cell differentiation on scaffolds with differing compositions and processing histories to determine how changes in chemical and thermomechanical properties influence biological response. Assessing mechanotransduction signaling pathways and downstream gene expression would provide deeper insight into how scaffold design affects cellular behavior and tissue-specific outcomes.

References

1. Ballen, K. K., Gluckman, E. & Broxmeyer, H. E. Umbilical cord blood transplantation: the first 25 years and beyond. *Blood* vol. 122 491–498 Preprint at https://doi.org/10.1182/blood-2013-02-453175 (2013).

2. Almouemen, N., Kelly, H. M. & O'Leary, C. Tissue Engineering: Understanding the Role of Biomaterials and Biophysical Forces on Cell Functionality Through Computational and Structural Biotechnology Analytical Methods. *Computational and Structural Biotechnology Journal* vol. 17 591–598 Preprint at https://doi.org/10.1016/j.csbj.2019.04.008 (2019).

3. *Biomaterials & Scaffolds for Tissue Engineering*. (2011).

4. Gattazzo, F., Urciuolo, A. & Bonaldo, P. Extracellular matrix: A dynamic microenvironment for stem cell niche. *Biochimica et Biophysica Acta - General Subjects* vol. 1840 2506–2519 Preprint at https://doi.org/10.1016/j.bbagen.2014.01.010 (2014).

5. Frantz, C., Stewart, K. M. & Weaver, V. M. The extracellular matrix at a glance. *Journal of Cell Science* vol. 123 4195–4200 Preprint at https://doi.org/10.1242/jcs.023820 (2010).

6. Smith, L. R., Cho, S. & Discher, D. E. Stem cell differentiation is regulated by extracellular matrix mechanics. *Physiology* vol. 33 16–25 Preprint at https://doi.org/10.1152/physiol.00026.2017 (2018).

7. Guilak, F. *et al.* Control of Stem Cell Fate by Physical Interactions with the Extracellular Matrix. *Cell Stem Cell* vol. 5 17–26 Preprint at https://doi.org/10.1016/j.stem.2009.06.016 (2009).

8. Engler, A. J., Sen, S., Sweeney, H. L. & Discher, D. E. Matrix Elasticity Directs Stem Cell Lineage Specification. *Cell* **126**, 677–689 (2006).

9. Zhang, X. *et al.* Harnessing matrix stiffness to engineer a bone marrow niche for hematopoietic stem cell rejuvenation. *Cell Stem Cell* **30**, 378-395.e8 (2023).

10. Dupont, S. *et al.* Role of YAP/TAZ in mechanotransduction. *Nature* **474**, 179–184 (2011).

11. Choi, J. S. & Harley, B. A. C. *B I O E N G I N E E R I N G Marrow-Inspired Matrix Cues Rapidly Affect Early Fate Decisions of Hematopoietic Stem and Progenitor Cells*.

12. Krishani, M., Shin, W. Y., Suhaimi, H. & Sambudi, N. S. Development of Scaffolds from Bio-Based Natural Materials for Tissue Regeneration Applications: A Review. *Gels* vol. 9 Preprint at https://doi.org/10.3390/gels9020100 (2023).

13. Amukarimi, S. & Mozafari, M. Biodegradable magnesium-based biomaterials: An overview of challenges and opportunities. *MedComm* vol. 2 123–144 Preprint at https://doi.org/10.1002/mco2.59 (2021).

14. Alonzo, M. *et al.* Bone tissue engineering techniques, advances, and scaffolds for treatment of bone defects. *Current Opinion in Biomedical Engineering* vol. 17 Preprint at https://doi.org/10.1016/j.cobme.2020.100248 (2021).

15. Chattopadhyay, S. & Raines, R. T. Review collagen-based biomaterials for wound healing. *Biopolymers* vol. 101 821–833 Preprint at https://doi.org/10.1002/bip.22486 (2014).

16. Harley, B. A., Leung, J. H., Silva, E. C. C. M. & Gibson, L. J. Mechanical characterization of collagen-glycosaminoglycan scaffolds. *Acta Biomater.* **3**, (2007).

17. Belbachir, K., Noreen, R., Gouspillou, G. & Petibois, C. Collagen types analysis and differentiation by FTIR spectroscopy. *Anal. Bioanal. Chem.* **395**, (2009).

18. Naomi, R., Ridzuan, P. M. & Bahari, H. Current insights into collagen type i. *Polymers* vol. 13 Preprint at https://doi.org/10.3390/polym13162642 (2021).

19. Elias, J., Matheson, B. A. & Gower, L. Influence of Crosslinking Methods on Biomimetically Mineralized Collagen Matrices for Bone-like Biomaterials. *Polymers (Basel).* **15**, (2023).

20. Yang, L., van der Werf, K. O., Dijkstra, P. J., Feijen, J. & Bennink, M. L. Micromechanical analysis of native and cross-linked collagen type I fibrils supports the existence of microfibrils. *J. Mech. Behav. Biomed. Mater.* **6**, 148–158 (2012).

21. Delgado, L. M., Pandit, A. & Zeugolis, D. I. Influence of sterilisation methods on collagen-based devices stability and properties. *Expert Review of Medical Devices* vol. 11 Preprint at https://doi.org/10.1586/17434440.2014.900436 (2014).

22. Iso. *COPYRIGHT PROTECTED DOCUMENT Published in Switzerland*. (2019).

23. Chen, Z. *et al.* Comparison of the properties of collagen–chitosan scaffolds after γ-ray irradiation and carbodiimide cross-linking. *J. Biomater. Sci. Polym. Ed.* **27**, (2016).

24. Delgado, L. M., Fuller, K. & Zeugolis, D. I. Influence of Cross-Linking Method and Disinfection/Sterilization Treatment on the Structural, Biophysical, Biochemical, and Biological Properties of Collagen-Based Devices. *ACS Biomater. Sci. Eng.* **4**, 2739–2747 (2018).

25. Monaco, G., Cholas, R., Salvatore, L., Madaghiele, M. & Sannino, A. Sterilization of collagen scaffolds designed for peripheral nerve regeneration: Effect on microstructure, degradation and cellular colonization. *Materials Science and Engineering C* **71**, 335–344 (2017).

26. Delgado, L. M., Pandit, A. & Zeugolis, D. I. Influence of sterilisation methods on collagen-based devices stability and properties. *Expert Review of Medical Devices* vol. 11 Preprint at https://doi.org/10.1586/17434440.2014.900436 (2014).

27. Gattazzo, F., Urciuolo, A. & Bonaldo, P. Extracellular matrix: A dynamic microenvironment for stem cell niche. *Biochimica et Biophysica Acta - General Subjects* vol. 1840 2506–2519 Preprint at https://doi.org/10.1016/j.bbagen.2014.01.010 (2014).

28. Guilak, F. *et al.* Control of Stem Cell Fate by Physical Interactions with the Extracellular Matrix. *Cell Stem Cell* vol. 5 17–26 Preprint at https://doi.org/10.1016/j.stem.2009.06.016 (2009).

29. Zhang, X. & Yue, R. Stiffness matters: A soft bone marrow organoid rejuvenates hematopoietic stem cells. *Mechanobiology in Medicine* vol. 1 Preprint at https://doi.org/10.1016/j.mbm.2023.100009 (2023).

30. Engler, A. J., Sen, S., Sweeney, H. L. & Discher, D. E. Matrix Elasticity Directs Stem Cell Lineage Specification. *Cell* **126**, 677–689 (2006).

31. Gurumurthy, B. & Janorkar, A. V. Improvements in mechanical properties of collagen-based scaffolds for tissue engineering. *Current Opinion in Biomedical Engineering* vol. 17 Preprint at https://doi.org/10.1016/j.cobme.2020.100253 (2021).

32. Alonzo, M. *et al.* Bone tissue engineering techniques, advances, and scaffolds for treatment of bone defects. *Current Opinion in Biomedical Engineering* vol. 17 Preprint at https://doi.org/10.1016/j.cobme.2020.100248 (2021).

33. Smith, L. R., Cho, S. & Discher, D. E. Stem cell differentiation is regulated by extracellular matrix mechanics. *Physiology* vol. 33 16–25 Preprint at https://doi.org/10.1152/physiol.00026.2017 (2018).

34. Roberts, T. T. & Rosenbaum, A. J. Bone grafts, bone substitutes and orthobiologics the bridge between basic science and clinical advancements in fracture healing. *Organogenesis* **8**, 114–124 (2012).

35. Huang, L. *et al.* Biomimetic Scaffolds for Tendon Tissue Regeneration. *Biomimetics* vol. 8 Preprint at https://doi.org/10.3390/biomimetics8020246 (2023).

36. Zhao, X. *et al.* Applications of Biocompatible Scaffold Materials in Stem Cell-Based Cartilage Tissue Engineering. *Frontiers in Bioengineering and Biotechnology* vol. 9 Preprint at https://doi.org/10.3389/fbioe.2021.603444 (2021).

37. Fendi, F., Abdullah, B., Suryani, S., Usman, A. N. & Tahir, D. Development and application of hydroxyapatite-based scaffolds for bone tissue regeneration: A systematic literature review. *Bone* vol. 183 Preprint at https://doi.org/10.1016/j.bone.2024.117075 (2024).

38. Gerhardt, L. C. & Boccaccini, A. R. Bioactive glass and glass-ceramic scaffolds for bone tissue engineering. *Materials* **3**, 3867–3910 (2010).

39. Vaiani, L. *et al.* Ceramic Materials for Biomedical Applications: An Overview on Properties and Fabrication Processes. *Journal of Functional Biomaterials* vol. 14 Preprint at https://doi.org/10.3390/jfb14030146 (2023).

40. Sonowal, L., Gautam, S., Mambiri, L. T. & Depan, D. Advancements of bioceramics in biomedical applications. *Next Materials* vol. 9 Preprint at https://doi.org/10.1016/j.nxmate.2025.101010 (2025).

41. Kumar, P., Dehiya, B. S. & Sindhu, A. *Bioceramics for Hard Tissue Engineering Applications: A Review*. *International Journal of Applied Engineering Research* vol. 13 http://www.ripublication.com (2018).

42. Ferreira, S. A., Young, G., Jones, J. R. & Rankin, S. Bioglass/carbonate apatite/collagen composite scaffold dissolution products promote human osteoblast differentiation. *Materials Science and Engineering C* **118**, (2021).

43. Ielo, I., Calabrese, G., De Luca, G. & Conoci, S. Recent Advances in Hydroxyapatite-Based Biocomposites for Bone Tissue Regeneration in Orthopedics. *International Journal of Molecular Sciences* vol. 23 Preprint at https://doi.org/10.3390/ijms23179721 (2022).

44. Abolhasani, S., Ahmadi, Y., Rostami, Y., Baravar, E. & Fattahi, D. Biomaterials in tissue repair and regeneration: key insights from extracellular matrix biology. *Frontiers in Medical Technology* vol. 7 Preprint at https://doi.org/10.3389/fmedt.2025.1565810 (2025).

45. Fan, J. *et al.* A Review of Recent Advances in Natural Polymer-Based Scaffolds for Musculoskeletal Tissue Engineering. *Polymers* vol. 14 Preprint at https://doi.org/10.3390/polym14102097 (2022).

46. Chen, M. *et al.* Natural polymer-based scaffolds for soft tissue repair. *Frontiers in Bioengineering and Biotechnology* vol. 10 Preprint at https://doi.org/10.3389/fbioe.2022.954699 (2022).

47. Sathiya, K., Ganesamoorthi, S., Mohan, S., Shanmugavadivu, A. & Selvamurugan, N. Natural polymers-based surface engineering of bone scaffolds – A review. *International Journal of Biological Macromolecules* vol. 282 Preprint at https://doi.org/10.1016/j.ijbiomac.2024.136840 (2024).

48. Chen, M. *et al.* Natural polymer-based scaffolds for soft tissue repair. *Frontiers in Bioengineering and Biotechnology* vol. 10 Preprint at https://doi.org/10.3389/fbioe.2022.954699 (2022).

49. Sathiya, K., Ganesamoorthi, S., Mohan, S., Shanmugavadivu, A. & Selvamurugan, N. Natural polymers-based surface engineering of bone scaffolds – A review. *International*

Journal of Biological Macromolecules vol. 282 Preprint at https://doi.org/10.1016/j.ijbiomac.2024.136840 (2024).

50. Chattopadhyay, S. & Raines, R. T. Review collagen-based biomaterials for wound healing. *Biopolymers* vol. 101 821–833 Preprint at https://doi.org/10.1002/bip.22486 (2014).

51. *Biomaterials & Scaffolds for Tissue Engineering*. (2011).

52. Frantz, C., Stewart, K. M. & Weaver, V. M. The extracellular matrix at a glance. *Journal of Cell Science* vol. 123 4195–4200 Preprint at https://doi.org/10.1242/jcs.023820 (2010).

53. Shoulders, M. D. & Raines, R. T. Collagen structure and stability. *Annual Review of Biochemistry* vol. 78 Preprint at https://doi.org/10.1146/annurev.biochem.77.032207.120833 (2009).

54. Daamen, W. F., Veerkamp, J. H., van Hest, J. C. M. & van Kuppevelt, T. H. Elastin as a biomaterial for tissue engineering. *Biomaterials* vol. 28 4378–4398 Preprint at https://doi.org/10.1016/j.biomaterials.2007.06.025 (2007).

55. Wise, S. G. & Weiss, A. S. Tropoelastin. *International Journal of Biochemistry and Cell Biology* vol. 41 494–497 Preprint at https://doi.org/10.1016/j.biocel.2008.03.017 (2009).

56. Augst, A. D., Kong, H. J. & Mooney, D. J. Alginate hydrogels as biomaterials. *Macromol. Biosci.* **6**, 623–633 (2006).

57. Lee, K. Y. & Mooney, D. J. Alginate: Properties and biomedical applications. *Progress in Polymer Science (Oxford)* vol. 37 106–126 Preprint at https://doi.org/10.1016/j.progpolymsci.2011.06.003 (2012).

58. Tomić, S. L. *et al.* Alginate-Based Hydrogels and Scaffolds for Biomedical Applications. *Marine Drugs* vol. 21 Preprint at https://doi.org/10.3390/md21030177 (2023).

59. Strus, B. & Szterk, A. PLGA-PEG-PLGA Polymer: From Synthesis to Advanced Pharmaceutical Applications. *Advances in Polymer Technology* vol. 2025 Preprint at https://doi.org/10.1155/adv/8899828 (2025).

60. Hussain, M., Khan, S. M., Shafiq, M. & Abbas, N. A review on PLA-based biodegradable materials for biomedical applications. *Giant* vol. 18 Preprint at https://doi.org/10.1016/j.giant.2024.100261 (2024).

61. Strus, B. & Szterk, A. PLGA-PEG-PLGA Polymer: From Synthesis to Advanced Pharmaceutical Applications. *Advances in Polymer Technology* vol. 2025 Preprint at https://doi.org/10.1155/adv/8899828 (2025).

62. Zhao, X. *et al.* Applications of Biocompatible Scaffold Materials in Stem Cell-Based Cartilage Tissue Engineering. *Frontiers in Bioengineering and Biotechnology* vol. 9 Preprint at https://doi.org/10.3389/fbioe.2021.603444 (2021).

63. Kutikov, A. B. & Song, J. Biodegradable PEG-Based Amphiphilic Block Copolymers for Tissue Engineering Applications. *ACS Biomater. Sci. Eng.* **1**, 463–480 (2015).

64. Zhang, Z. *et al.* A review of preparation methods of porous skin tissue engineering scaffolds. *Materials Today Communications* vol. 32 Preprint at https://doi.org/10.1016/j.mtcomm.2022.104109 (2022).

65. Kumar, A. & Jacob, A. Techniques in scaffold fabrication process for tissue engineering applications: A review. *Journal of Applied Biology and Biotechnology* vol. 10 163–176 Preprint at https://doi.org/10.7324/JABB.2022.100321 (2022).

66. Lutzweiler, G., Halili, A. N. & Vrana, N. E. The overview of porous, bioactive scaffolds as instructive biomaterials for tissue regeneration and their clinical translation. *Pharmaceutics* vol. 12 1–29 Preprint at https://doi.org/10.3390/pharmaceutics12070602 (2020).

67. Santos-Rosales, V., Iglesias-Mejuto, A. & García-González, C. A. Solvent-free approaches for the processing of scaffolds in regenerative medicine. *Polymers* vol. 12 Preprint at https://doi.org/10.3390/polym12030533 (2020).

68. Yang, C. *Enhanced Physicochemical Properties of Collagen by Using EDC/NHS-Crosslinking*. *Bull. Mater. Sci* vol. 35 (2012).

69. Grover, C. N. *et al.* Crosslinking and composition influence the surface properties, mechanical stiffness and cell reactivity of collagen-based films. *Acta Biomater.* **8**, 3080–3090 (2012).

70. Jiang, Y.-H. *et al. Cross-Linking Methods of Type I Collagen-Based Scaffolds for Cartilage Tissue Engineering*. *Am J Transl Res* vol. 14 www.ajtr.org (2022).

71. Schyra, P., Aibibu, D., Sundag, B. & Cherif, C. Chemical Crosslinking of Acid Soluble Collagen Fibres. *Biomimetics* vol. 10 Preprint at https://doi.org/10.3390/biomimetics10100701 (2025).

72. Muhamad, N. & Zaidel, D. N. A. Enhancing collagen functionality through chemical, physical, and enzymatic modification strategies: review. *Polymer Bulletin* vol. 83 Preprint at https://doi.org/10.1007/s00289-026-06457-8 (2026).

73. Yang, C. *Enhanced Physicochemical Properties of Collagen by Using EDC/NHS-Crosslinking*. *Bull. Mater. Sci* vol. 35 (2012).

74. Patel, J. M., Jackson, R. C., Schneider, G. L., Ghodbane, S. A. & Dunn, M. G. Carbodiimide cross-linking counteracts the detrimental effects of gamma irradiation on the physical properties of collagen-hyaluronan sponges. *J. Mater. Sci. Mater. Med.* **29**, (2018).

75. Chen, Z. *et al.* Comparison of the properties of collagen–chitosan scaffolds after γ-ray irradiation and carbodiimide cross-linking. *J. Biomater. Sci. Polym. Ed.* **27**, 937–953 (2016).

76. Delgado, L. M., Pandit, A. & Zeugolis, D. I. Influence of sterilisation methods on collagen-based devices stability and properties. *Expert Review of Medical Devices* vol. 11 305–314 Preprint at https://doi.org/10.1586/17434440.2014.900436 (2014).

77. Monaco, G., Cholas, R., Salvatore, L., Madaghiele, M. & Sannino, A. Sterilization of collagen scaffolds designed for peripheral nerve regeneration: Effect on microstructure, degradation and cellular colonization. *Materials Science and Engineering C* **71**, 335–344 (2017).

78. Tao, M. *et al.* Sterilization and disinfection methods for decellularized matrix materials: Review, consideration and proposal. *Bioactive Materials* vol. 6 2927–2945 Preprint at https://doi.org/10.1016/j.bioactmat.2021.02.010 (2021).

79. Delgado, L. M., Fuller, K. & Zeugolis, D. I. Influence of Cross-Linking Method and Disinfection/Sterilization Treatment on the Structural, Biophysical, Biochemical, and Biological Properties of Collagen-Based Devices. *ACS Biomater. Sci. Eng.* **4**, 2739–2747 (2018).

80. Grieb, T. *et al.* Effective use of gamma irradiation for pathogen inactivation of monoclonal antibody preparations. *Biologicals* **30**, 207–216 (2002).

81. Qin, J. *et al.* Impact of Co-60 γ-ray irradiation on the cross-linking and stability of fish collagen: Structural changes and digestibility. *Food Hydrocoll.* **157**, (2024).

82. Tuieng, R. J. *et al.* Impact of therapeutic X-ray exposure on collagen I and associated proteins. *Acta Biomater.* **197**, 294–311 (2025).

83. Sauer, K. *et al.* Primary radiation damage in bone evolves via collagen destruction by photoelectrons and secondary emission self-absorption. *Nat. Commun.* **13**, (2022).

84. Chlup, H., Suchý, T. & Šupová, M. The electron beam induced cross-linking of bovine collagen gels with various concentrations: The mechanical properties and secondary structure. *Polymer (Guildf).* **287**, (2023).

85. Ng, K. *et al.* Effects of Ionizing Radiation on the Biophysical Properties of Type I Collagen Fibrils. *PLoS One* **20**, (2025).

86. Terzi, A. *et al.* Effects of processing on structural, mechanical and biological properties of collagen-based substrates for regenerative medicine. *Sci. Rep.* **8**, (2018).

87. Cheung, D. T., Perelman, N., Tong, D. & Nimni, M. E. The effect of γ-irradiation on collagen molecules, isolated α-chains, and crosslinked native fibers. *J. Biomed. Mater. Res.* **24**, 581–589 (1990).

88. Annor, A. H. *et al.* Effect of enzymatic degradation on the mechanical properties of biological scaffold materials. *Surg. Endosc.* **26**, 2767–2778 (2012).

89. Jafari-Sabet, M., Nasiri, H. & Ataee, R. The Effect of Cross-Linking Agents and Collagen Concentrations on Properties of Collagen Scaffolds. *Journal of Archives in Military Medicine* **4**, (2016).

90. Patel, J. M., Jackson, R. C., Schneider, G. L., Ghodbane, S. A. & Dunn, M. G. Carbodiimide cross-linking counteracts the detrimental effects of gamma irradiation on the physical properties of collagen-hyaluronan sponges. *J. Mater. Sci. Mater. Med.* **29**, (2018).

91. Kyriakidou, M. *et al. An FT-IR Spectral Analysis of the Effects of γ-Radiation on Normal and Cancerous Cartilage*.

92. Abraham, L. C., Zuena, E., Perez-Ramirez, B. & Kaplan, D. L. Guide to collagen characterization for biomaterial studies. *Journal of Biomedical Materials Research - Part B Applied Biomaterials* vol. 87 264–285 Preprint at https://doi.org/10.1002/jbm.b.31078 (2008).

93. Murphy, C. M., Haugh, M. G. & O'Brien, F. J. The effect of mean pore size on cell attachment, proliferation and migration in collagen-glycosaminoglycan scaffolds for bone tissue engineering. *Biomaterials* **31**, (2010).

94. Sahadat Hossain, M. & Ahmed, S. FTIR spectrum analysis to predict the crystalline and amorphous phases of hydroxyapatite: a comparison of vibrational motion to reflection. *RSC Adv.* **13**, 14625–14630 (2023).

95. Parenteau-Bareil, R., Gauvin, R. & Berthod, F. Collagen-based biomaterials for tissue engineering applications. *Materials* **3**, 1863–1887 (2010).

96. Kim, S. Y. *et al.* L-Serine–Incorporated Collagen Scaffolds for Modulating In Vivo Degradation Behavior. *J. Funct. Biomater.* **16**, (2025).

97. Sahadat Hossain, M. & Ahmed, S. FTIR spectrum analysis to predict the crystalline and amorphous phases of hydroxyapatite: a comparison of vibrational motion to reflection. *RSC Adv.* **13**, 14625–14630 (2023).

98. Liu, Y. xin *et al.* Effects of collagenase type I on the structural features of collagen fibres from sea cucumber (Stichopus japonicus) body wall. *Food Chem.* **301**, (2019).

99. Shi, L., Ermis, R., Garcia, A., Telgenhoff, D. & Aust Shi, D. L. *Degradation of Human Collagen Isoforms by Clostridium Collagenase and the Effects of Degradation Products on Cell Migration Degradation of Human Collagen Isoforms by Clotridium Collagenase and the Effects of Degradation Products on Cell Migration*. *Int Wound J* vol. 7 (2010).

100. Hernández, B. *et al.* Structural Analysis of Nonapeptides Derived from Elastin. *Biophys. J.* **118**, 2755–2768 (2020).

101. Nguyen, N. K., Leoni, M., Maniglio, D. & Migliaresi, C. Hydroxyapatite nanorods: Soft-template synthesis, characterization and preliminary in vitro tests. *J. Biomater. Appl.* **28**, 49–61 (2013).

102. Faraj, K. A. *et al. The Effect of Ethylene Oxide Sterilisation, Beta Irradiation and Gamma Irradiation on Collagen Fibril-Based Scaffolds*. *Tissue Engineering and Regenerative Medicine* vol. 8 (2011).

103. Bublikova, A., Schütte, F. & Mayr, S. G. Programming fibril alignment and mechanical response in reconstituted collagen fibers using reagent-free biomimetic energetic electron crosslinking. *Mater. Adv.* **5**, 4807–4817 (2024).

104. Zeugolis, D. I. & Raghunath, M. The physiological relevance of wet versus dry differential scanning calorimetry for biomaterial evaluation: A technical note. *Polym. Int.* **59**, 1403–1407 (2010).